# Thermodynamics of amyloid fibril growth from non-equilibrium experiments of growth and dissociation

Rasmus K. Norrild*

*Technical University of Denmark, Department of Biotechnology and Biomedicine*

Nicola Vettore*

*Technical University of Denmark, Department of Biotechnology and Biomedicine*

Alberto Coden*

*Technical University of Denmark, Department of Biotechnology and Biomedicine*

Wei-Feng Xue

*School of Biosciences, University of Kent*

Alexander K. Buell[1]

*Technical University of Denmark, Department of Biotechnology and Biomedicine*

**These authors contributed equally to the work*

**Abstract**

Amyloid fibrils are ordered, non-covalent polymers of proteins that are linked to a range of diseases, as well as biological functions. Amyloid fibrils are often considered thermodynamically so stable that they appear to be irreversible, explaining why very few quantitative thermodynamic studies have been performed on amyloid fibrils, compared to the very large body of kinetic studies. Here we explore the thermodynamics of amyloid fibril formation by the protein PI3K-SH3, which forms amyloid fibrils under acidic conditions. We use quartz crystal microbalance (QCM) and develop novel temperature perturbation experiments based on differential scanning fluorimetry (DSF) to quantify the temperature dependence of the fibril growth and dissociation rates, allowing us to quantitatively describe the thermodynamic stability of the fibrils between 10 and 70°C.

[1]to whom correspondence should be addressed: alebu@dtu.dk

This amyloid system is characterised by a moderate temperature dependence of the fibril growth rate and a strong temperature dependence of the dissociation rate, leading to a measurable increase in solubility above approximately 50°C.
*Keywords:* amyloid, kinetics, thermodynamics, non-equilibrium system, biosensing, differential scanning fluorimetry, quartz crystal microbalance

---

## Introduction

Amyloid fibrils are highly ordered polymers of proteins and peptides. These structures have received much attention in the last two decades because of their being the hallmark of a wide range of different human disorders, most notably some devastating neurodegenerative diseases, e.g. Alzheimer's and Parkinson's. At the same time, amyloid fibrils play also functional roles in biology, as templates [1], as storage forms of peptide hormones [2], or for structural integrity, e.g. in bacterial biofilms [3]. In addition to the functional and disease-related amyloid proteins, many additional proteins have been found to form amyloid fibrils under certain sets of solution conditions. One such protein is the Src-homology 3 domain of phosphatidyl-inositol-3-kinase (PI3K-SH3). A stably folded small protein at neutral pH [4], it transforms into amyloid fibrils at acidic pH, which destabilises its native fold [5]. This protein has played an extraordinarily important role in the history of amyloid research. It was during studies of protein folding mechanisms [6] that the group of Sir Chris Dobson discovered the amyloid-forming potential of PI3K-SH3 [7], when an acidic solution of the protein was left in an NMR tube for several days was found to have transformed into a gel. A range of seminal studies that revealed fundamental features of the amyloid state were performed on the PI3K-SH3 system. Examples include studies that established the cellular toxicity potential of early aggregate species on the pathway to amyloid fibril formation [8] and method developments to measure the time evolution of oligomer populations [9]. Also some of the earliest amyloid structural biology was performed on PI3K-SH3 fibrils, ranging from cryo-electron microscopy [10], limited proteolysis [11] to

solid state NMR spectroscopy [12]. Indeed, the discovery that PI3K-SH3 can form amyloid fibrils has significantly contributed to the birth of the generic amyloid hypothesis, the intellectual father and most prominent proponent of which was Sir Chris Dobson [13, 14]. This hypothesis states that polypeptides are substances with inherently limited solubility and that the amyloid state is a thermodynamically stable insoluble state that is accessible to many different polypeptide sequences, ranging from very short peptides to large proteins. The question about the mechanisms and driving forces for the transformation of soluble protein into amyloid fibrils has been the subject of intense investigation in recent years. Most of the focus has been put on kinetic and mechanistic aspects of this transition, while the question as to the origin and magnitude of the thermodynamic stability of amyloid fibrils has received less attention. Amyloid fibrils of many proteins appear to be virtually irreversible under physiologically relevant conditions, both *in vitro* and *in vivo*, which explains the lack of quantitative data on their thermodynamic stability. It has, however, been shown that amyloid fibrils can be dissolved with strong chemical denaturants [15, 16, 17, 18], as well as by exposing them to high temperatures [19, 20, 21, 22, 23, 24]. The amyloid fibrils from a range of proteins have been characterised by chemical denaturation and it has been found that absolute stability increases with sequence length, but stability per amino acid is highest for short sequences [16]. Insight into the thermodynamics of the amyloid state can also be obtained from measurements of fibril growth and dissociation rates. It can be shown (see supplementary materials) that the ratio of the dissociation and growth rate constants corresponds to the equilibrium concentration of monomer, which is a measure of fibril stability - the smaller the concentration of monomer at equilibrium, the more stable the fibrils. Such an analysis has been performed for example for the amyloid beta peptide, both through direct measurements of the equilibrium concentration of monomer [25, 26], as well as from measurements of fibril growth and dissociation kinetics by surface plasmon resonance (SPR) [27]. To our knowledge, no amyloid system has so far been thermodynamically characterised by both chemical denaturation, as well as by measurements of growth

and dissociation rates, and the resulting stabilities compared. We have recently presented an in-depth analysis of the equilibrium chemical depolymerization of PI3K-SH3 [17], which led to the conclusion that the standard isodesmic linear polymerization model (a single equilibrium constant) is incomplete and only an extended version, the cooperative linear polymerization model (two equilibrium constants, of nucleation and growth), is able to fully reproduce all features of the chemical depolymerization experiments. In the present work, we measure the temperature dependence of both the growth and dissociation rate constants of PI3K-SH3 amyloid fibrils and from this data define the temperature-dependent thermodynamic stability of these fibrils. We study the response of the fibril system initially in equilibrium with monomer after perturbation by both changes in monomer concentration as well as temperature. In particular, we introduce a new method, whereby differential scanning fluorimetry is used to monitor the response of the fibril system upon sudden (T-jump) or continuous (T-ramp) changes in temperature. While the T-jump perturbation method of chemical systems was originally developed for ultra-fast reactions [28], we show that it can also be of benefit in the case of slowly relaxing systems, such as amyloid fibrils.

## Materials and Methods

*Protein production, purification and conversion into amyloid fibrils*

*Protein expression*

RosettaTM(DE3) *E.coli* Competent Cells (Novagen) transfected with a pET-14b Vector (Novagen) coding for the PI3K-SH3 domain fused to an histidine tag were used for the protein production. Six liters of inducing media were prepared according to the following protocol: dissolution of 24g/l yeast extract, 12g/l tryptone and 6 ml/l of glycerol (Carl Roth GmbH + Co. KG, Karsruhe, Germany) in 5400 ml of deionized water and sterilization in autoclave. After cooling down the media, a total of 600 ml of a separately-sterilized solution of 0.17 M $KH_2PO_4$ (Gürssing GmbH Analytica, Filsum, Germany), 0.72

M $K_2HPO_4$ (Carl Roth GmbH + Co. KG, Karsruhe, Germany) were added, as well as 6 ml/l of a 10% glucose (Sigma-Aldrich, Merck KGaA, Darmstadt, Germany) solution, 30 ml/l of a 8% lactose (Carl Roth GmbH + Co. KG, Karsruhe, Germany) solution (both of them sterilized by filtration with a 0.22 $\mu$m cut-off filter) and 100 mg/ml ampicillin (Thermofisher Scientific, Waltham, Massachusetts, USA). The growth medium was then transferred into four 5 liter flasks, inoculated, and grown overnight at 37℃ under 120 rpm agitation in a Infors Multitron Standard shaker.

*Protein purification*

After the incubation overnight, the culture was subjected to 20 minutes of centrifugation at 4℃ at 5000 g in a JLA 10500 rotor. The supernatant was then discarded, and the cells re-suspended in a 50 mM phosphate buffer with 10mM NaCl (Fisher Scientific UK, Leics, United Kingdom), 5 mM imidazole (Sigma-Aldrich, Merck KGaA, Darmstadt, Germany) solution at pH 8.0. Three EDTA-free protease inhibitor tablets (Roche, Grenzach-Wyhlen, Germany) were then dissolved in 1 ml buffer and added to the solution, together with 150 $\mu$l of a 10 mg/ml DNAse solution (Sigma-Aldrich, Merck KGaA, Darmstadt, Germany). Sonication with a VS 70 T probe was then carried out for 10 minutes (3s pulse, 5s pause) at 40% amplitude. After 1h of centrifugation at 4℃ at 1800 rpm with a JA 20 rotor, the solution was frozen and stored at -20℃. Before the chromatographic purification, the solution was thawed and filtrated with a 0.22 $\mu$m cut-off filter. Immoblized metal affinity chromatography (IMAC) was performed, in order to separate the protein from the rest of the lysate. This procedure utilized a HisTrapTMFF column with immobilized nickel on a agarose resin (NiSepharoseTMFastFlow), in order to retain the recombinant PI3K-SH3 domain through the fused histidine tag. A gradient of two solutions was utilized: A) 50 mM Phosphate buffer, 10 mM NaCl, 5 mM imidazole solution at pH 8.0, B) 50 mM Phosphate buffer, 10 mM NaCl, 100 mM imidazole solution at pH 8.0. The flow rate was set to 1.5ml/min, and the gradient was set to go from 0 to 100% of solution B in 50ml. After the collection, the samples were

incubated overnight with a solution of Trypsin (Sigma-Aldrich, Merck KGaA, Darmstadt, Germany) at 4℃ under agitation, in order cleave off the hystidine tag. Size-exclusion chromatography (SEC) was then carried out with an ÄKTA Pure apparatus, equipped with a HiLoadTM26/60 SuperdexTM75 prep grade cross-linked agarose and dextran column, equilibrated with 5 mM ammonium acetate (Carl Roth GmbH + Co. KG, Karsruhe, Germany) buffer at pH 7. The previously obtained fractions derived from the IMAC where concentrated with a Vivaspin ® 20 membrane with 10 kDa cut-off, under centrifugation at 8000 rpm for 30 minutes prior to the injection in the SEC column. 5 ml of solution were injected for each chromatographic run. Each collected fraction was run in an SDS-PAGE, in order to evaluate the identity and the purity of the product. The fractions obtained from the SEC purification were flash-frozen with liquid nitrogen and lyophilized. The dry protein was stored at -20℃.

*Amyloid fibril preparation*

PI3K-SH3 amyloid fibrils were prepared at pH 2. For the QCM experiments, they were prepared in 10 mM HCl, whereas for the DSF experiments, they were prepared in 10 mM glycine-HCl buffer (pH 2). The reason for this difference is that the presence of the glycine buffer interferes with the chemical modification of the fibrils required for the attachment to the QCM sensor, see below. In both cases, fibrils were obtained by incubation of 300-450 $\mu$M PI3K-SH3 protein solutions for 4 days at 42℃ under agitation. Protein concentrations were measured by absorbance spectroscopy, using an extinction coefficient of 15930 $M^{-1}cm^{-1}$ at 280 nm. Subsequent generations of fibrils were always seeded with a small percentage of the previous generation. Over the course of our experiments, 8 generation of fibrils were prepared in the case of the glycine buffer.

*Atomic force microscopy (AFM) imaging*

The fibril samples (before and after sonication) were diluted with 10 mM HCl to a concentration of 1 or 2 $\mu$M. 5 $\mu$l were deposited on freshly cleaved mica and left to dry. The samples were subsequently imaged using a multimode

8 AFM with a Nanoscope V controller (Bruker) operating under peak force tapping in the ScanAsyst mode using Bruker ScanAsyst probes (silicon nitride triangular tip with nomina tip radius of 2 nm and nominal spring constant of 0.4 N/m). The height channel images, each with a scan size of 5 x 5 $\mu$m and 1024 x 1024 pixels were collected. Nanoscope analysis software (Version 1.5, Bruker) was used to process the image data by flattening the height topography data to remove tilt and bow.

*Quartz crystal microbalance (QCM) experiments*

The PI3K-SH3 amyloid fibrils were chemically modified by attaching cystamine, in order to allow attachment to the gold-coated sensor [29]. In brief, fibril functionalization was carried out by dissolving 0.023 g of cystamine dihydrochloride (Sigma-Aldrich, Merck KGaA, Darmstadt, Germany) in 100 $\mu$l of MilliQ water and by adding this solution to 200 $\mu$l of PI3K-SH3 fibrils in HCl pH 2 (see the section above for more details on fibril preparation). The whole volume was then directly added to 0.001 g of N-(3-Dimethylaminopropyl)-N'-ethylcarbodiimide hydrochloride (EDC; Sigma-Aldrich, Merck KGaA, Darmstadt, Germany) and vortexed. HCl pH 2 was then added until reaching a final volume of 1.5 ml. The sample was then subjected to 30 minutes of centrifugation at 16.1 krpm at 21°C. The supernatant was discarded and the precipitated fibrils resuspended into 1.5 ml of HCl pH 2. The centrifugation/re-suspension procedure was repeated three times, but after the third centrifugation the pellet was resuspended into 500 $\mu$l instead of 1.5 ml. This procedure is necessary in order to remove most of the un-reacted cystamine, that would otherwise compete for the attachment to the available gold surface. The obtained suspension of fibrils was then sonicated for 15 s (1 s pulse, 2s pause, at 10%amplitude) prior to the attachment of the fibrils to the sensor surface. Clean QCM sensors were incubated overnight with 150 $\mu$l of fuctionalized fibril suspension, under 100% humidity (in order to reduce the evaporation of the sample). Prior to the start of the QCM experiments, the sensors were rinsed extensively with HCl pH 2 and incubated with a 1:100 aqueous mPEG-thiol (PolyPure, Norway) solution for

30 minutes under 100% humidity, in order to passivate the remaining surface. After the incubation the sensors were rinsed with HCl pH 2, dried under nitrogen gas flow and placed in the QCM sensor chamber for the experiment. The measurements of the temperature and concentration dependencies of the fibril elongation rate was carried out by performing injections of monomer solutions in 10 mM glycine-HCl pH 2 buffer at different concentrations and temperatures, ranging from 10 to 70℃. Absolute rates obtained from different sensors cannot be directly compared, due to the potential differences in the surface concentration of the attached fibrils, which translate into different frequency responses upon injection of a given monomer concentration. Normalization of data obtained from different sensors is therefore mandatory in order to compose a single data set. This procedure is carried out by performing an injection of a solution with a specific monomer concentration at a specific temperature onto all the considered sensors. The rates of frequency change are then compared, a reference sensor is chosen and under the assumption that all measured rates under this set of conditions should be equal, a multiplicative factor is deduced with which to multiply all rates from sensors other than the reference sensor.

*Differential scanning fluorimetry (DSF) experiments*

DSF measurements were performed using a "Prometheus" instrument (Nanotemper, Munich, Germany). The instrument allows to measure the fluorescence emission intensity at 330 and 350 nm upon excitation at 280 nm, in microcapillaries. Measurements can be performed at constant temperature, upon rapid changes in temperature, or during temperature ramps at different rates. We have previously reported that in the case of PI3K-SH3 amyloid fibrils, intrinsic protein fluorescence is a convenient tool that allows to determine the relative concentrations of monomers and fibrils in a sample, because the tryptophan fluorescence is strongly quenched in the fibrillar state [17]. 440 $\mu$M PI3K-SH3 fibril stock solution was diluted to 100 $\mu$M before being sonicated using a Vial Tweeter sonication device (Hielscher Ultrasonics GmbH, Tieltow, Germany). 250 $\mu$l samples were sonicated on ice at maximum amplitude for 5 times 10

seconds resulting in approximately 500 J. The fibrils were then equilibrated over night before use. Approximately 10 $\mu$l fibril sample was filled through capillary action into high sensitivity (quartz) capillaries immediately before the measurements.

*Full fibril dissolution*

100 $\mu$M of non-sonicated fibrils were heated to 110℃ and subsequently cooled back to 20℃ at a rate of 1.5℃/min. A sample of 100 $\mu$M monomeric PI3K-SH3 was included as a reference.

*Temperature jump experiments*

For the measurements of growth rates at 15-40℃, the samples were equilibrated overnight at 40℃ after sonication. To release monomers from the fibrils, the samples were left to partly dissociate at 60℃ for 20 minutes before the temperature was rapidly lowered to the desired temperature at which the growth rate was to be measured. For the temperature jump experiments to high temperatures (60-75℃), the fibrils were incubated for several days at 15℃ to ensure slower kinetics. The experiments included an annealing strategy where the fibrils were partly dissociated at 75℃ for 5 minutes, regrown at 40℃ for 20 minutes, before finally changing the temperature to 60-75℃ and recording the change in fluorescence emission. The annealing made the experiments more reproducible and slowed down the reaction, possibly due to the dissolution of very short fibrils during the short period at 75℃ This renders the analysis more reliable, as the rate of dissociation is slowed down with fewer fibril ends, which makes the finite time it takes to reach the upper temperature less significant in the experiment. To extract the initial rates, the fraction of monomeric protein was estimated by including monomeric reference samples. The fibril fluorescence at high temperatures was extrapolated from ramping experiments where the temperature dependence of the fibrillar state can be approximated by a linear function before dissociation starts. The fraction of monomer was then calculated by subtracting the fibril signal from the measured data and after-

wards dividing by the fluorescence signal of the monomeric sample subtracted by the fibril sample. All the temperature jump experiments were performed at three different fibril concentrations (25, 50 and 100 $\mu$M), which corresponds to different numbers of growing and dissociating fibril ends.

*Temperature ramp experiments*

The temperature ramps were performed at different rates (0.5, 1 and 1.5℃ per minute) of 100 $\mu$M fibril samples. Prior to the ramp, the samples were equilibrated over night after sonication as desribed above before performing a short annealing (5 minutes at 65℃, 20 minutes at 40℃, and 30 minutes of equilibration at 15℃). The ramp was started at 15℃ and the upper temperature was kept constant at 65℃. Only the data above 40℃ was used in the fits, but the lower starting temperature of 15℃ was chosen in order to obtain a better-defined baseline (15-50℃) of the fibril fluorescence, facilitating extrapolation into the temperature region where the fibrils start to dissociate. A monomer reference sample was also included in order to be able to calculate the fraction of monomer as described above.

*Spectroscopic characterisation of fibrils*

UV-fluorescence spectra of 25 $\mu$M PI3K-SH3 amyloid fibrils in 10 mM glycine-HCl pH 2 were recorded before and after heat-induced dissociation at 90℃ for 10 minutes using a Probe drum instrument (Probation Labs, Lund, Sweden) in manual mode. The spectra were recorded at 25℃ using excitation with an 280 nm LED with an integration time of 200 ms and averaging over 64 measurements. Additionally, fibril concentration was checked by recording an absorbance spectrum on the denaturated sample.

*Data analysis and model fitting*

Data analysis and model fitting was performed with Python using the packages Numpy, Pandas, Matplotlib and Lmfit. Non-linear least squares analysis with Lmfit was performed using the Levenberg-Marquardt algortihm. All error

estimates given are directly from the covariance matrix. For the QCM data, the activation enthalpy of the fibril elongation rate was analysed in the temperature range 15-35℃ assuming negligible dissociation rate in this temperature range. The activation enthalpy of the elongation rate constant was kept constant when analysing the full data set. The same strategy was applied when analysing the larger data set at three different monomer concentrations. As an extension of this simple model, we included a heat capacity for the enthalpy of activation of the growth reaction. Single exponential functions were fitted to the temperature jump experiments, directly in fluorescence intensity units. The conversion of the fluorescence signal into absolute monomer concentrations was obtained by reference to a monomeric sample and an extrapolation of the base line of a purely fibrillar sample. The theoretical description of the T-ramp fitting can be found in supplementary section 6.

## Results

*Surface-based biosensing measurements of amyloid fibril growth by QCM*

We first performed an analysis of the temperature dependence of the absolute fibril growth rate of PI3K-SH3 amyloid fibrils over a wide temperature range (10-55℃, Figure 1) at a fixed concentration of 5 $\mu$M monomeric protein, using a quartz crystal microbalance (QCM). Details of the experimental procedures can be found in the methods section. The principle of the method is to attach pre-formed fibrils to the surface of a piezoelectric quartz disk and then monitor their growth upon incubation with monomeric protein via a change in the resonant frequency of the quartz disk. This method is particularly well-suited for evaluations of relative changes in amyloid fibril elongation rates, because the same ensemble of fibrils is repeatedly exposed to monomer solutions and therefore even small relative changes in elongation rate of a few tens of percent can be resolved [30]. Interestingly, we find a non-monotonic temperature dependence of the growth rate, with a decrease in rate above 40℃. Curvature in Arrhenius-plots of protein folding reactions at high temperatures are well-

established and generally interpreted as either stemming from the roughness of the free energy landscape of folding [31], as well as a non-negligible heat capacity associated with the transition state of the folding reaction [32, 33]. It has also been pointed out that curved Arrhenius-plots of protein folding can be linearised by ensuring iso-stability conditions [34]; in other words, the curvature stems from a significant increase in the back reaction, i.e. unfolding in the case of an Arrhenius-plot for folding. We noticed that the fibrils showed signs of dissociation (frequency increase) when in contact with buffer at the highest temperatures of our QCM experiments (50℃ and above). This observation suggests that the dissociation reaction significantly contributes to the data at the highest temperatures. In order to test whether a temperature-dependent combination of growth and dissociation is able to quantitatively describe the data, the signal from the QCM (rate of frequency change) needs to be converted into molecular units. If only fibril elongation contributes to the signal and the assumption holds that the rate of change of frequency is proportional to the fibril growth rate [35, 36], then the Arrhenius-plot can be performed directly on the raw data of rate of frequency shift. However, when the net rate, i.e. the sum of the growth and dissociation rates is measured:

$$A\frac{dF}{dt} = \frac{d[M]}{dt} = k_+[P]_{\mathrm{surf}}[m] - k_-[P]_{\mathrm{surf}} \tag{1}$$

where F is the resonant frequency, A is the mass sensitivity of the QCM sensor for fibril growth and [M] is the fibril mass attached to the sensor, then the surface concentration of fibrils, $[\mathrm{P}]_{\mathrm{surf}}$, needs to be estimated. We have $\frac{[M]}{[P]_{\mathrm{surf}}} = \mathrm{L}$, the average length of the fibrils in monomer units. We therefore obtain:

$$\frac{A}{[P]_{\mathrm{surf}}}\frac{dF}{dt} = \frac{dL}{dt} = k_+[m] - k_- \tag{2}$$

The rate constants $\mathrm{k}_+$ and $\mathrm{k}_-$ need to be in molar units, such that multiplication with the monomer concentration in molar units and subtraction of the two rates can be carried out. It is intrinsically difficult to provide an accurate

estimate for the surface concentration of fibrils, because the conditions of very high surface density of fibrils (see methods section and supplementary figure 3), required for experiments at low monomer concentrations, are also conditions that render it difficult to accurately estimate the fibril density. However, this does not affect the relative magnitudes of the rate constants and temperature dependencies of the growth and dissociation rates, as they both contain the fibril surface concentration. Indeed, we are able to fit a model consisting of a combination of growth and dissociation, with different activation energies, to the data. In the following, we treat the Arrhenius activation energy and the enthalpy of activation as equivalent, as it can be shown that they are very similar in magnitude for reactions in solution [37].

The activation energy we find for the growth reaction ($36.7 \pm 5.0$ kJ/mol) is in good agreement with the value we have reported previously ($42.9 \pm 8.5$ kJ/mol, [30]). We find that the dissociation reaction has a significantly higher activation energy than the growth reaction ($105.4 \pm 10.4$ kJ/mol), which explains why the dissociation reaction can be negligible at temperatures below ca. 40°C, but become significant at higher temperatures. If we use the kinetic pre-factors for fibril elongation and dissociation discussed in supplementary section 2, then we can also use the fit results to estimate the ratio of dissociation and growth rate constants, which corresponds formally to the equilibrium concentration, $\frac{k_-}{k_+} = c_{eq}$ in the limit of $[M] \gg c_{eq}$.

We obtain $c_{eq} = 0.5$ $\mu$M, corresponding to a free energy change of -36.2 kJ/mol for the fibrillar state with respect to the monomeric state at 28°C (using a hypothetical reference concentration of 1 M). We will discuss below how this value compares to estimates from our DSF experiments, as well as estimates of fibril stability from equilibrium denaturation experiments [17]. An important prediction of this model for the temperature dependence of amyloid fibril elongation is that Arrhenius-plots should display different degrees of curvature depending on the monomer concentration used, because only the elongation reaction and not the dissociation reaction depends on the monomer concentration, leading to a concentration-dependent balance between these two reactions. We

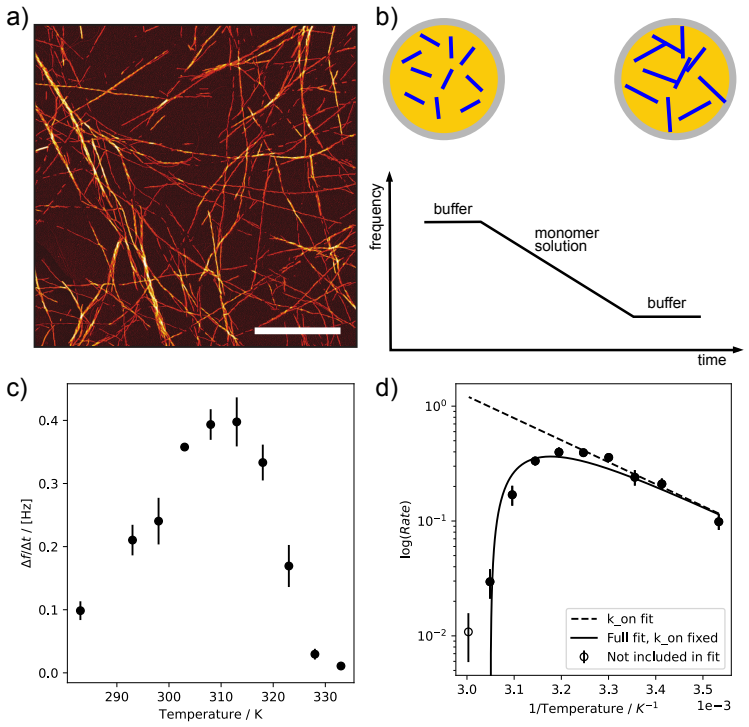


Figure 1: a) AFM image of PI3K-SH3 amyloid fibrils before sonication. Scale bar indicates 1 $\mu$m. b) Illustration of the principle of QCM measurements of amyloid fibril growth [35, 36]. The growth of surface-bound seed fibrils upon exposure to monomer solutions can be followed in real time through the decrease in resonant frequency. c) The rate of frequency change observed as a function of temperature for the overtone with N = 3, upon injection of a monomer solution at 5 $\mu$M. d) Arrhenius-plot of the data shown in c), with the linear fit at low temperatures indicated as an interrupted line, and the fit to the sum of growth and dissociation indicated as a continuous line.

tested this hypothesis by measuring the temperature dependence (10-60℃) of fibril growth at three different concentrations (4, 12 and 17 $\mu$M) and we indeed observe that at the lowest concentration and highest temperature, no net growth but dissociation is observed, whereas the two higher concentrations show clear net growth (supplementary figure 1). We fitted this data set globally, and were able to qualitatively reproduce the observed behaviour with the model described above, i.e. a combination of growth and dissociation. A significantly improved fit was obtained after adding an additional free parameter, a heat capacity for the enthalpy of activation of the growth reaction. Inclusion of a heat capacity for an activation enthalpy corresponds to a temperature dependence of the magnitude of the energy barrier. We discuss this choice of additional free parameter below.

In addition to measuring the temperature dependence of fibril growth at different concentrations, it is also possible to explore the concentration dependence in more detail for selected temperatures. In supplementary figure 2, we show the effects of variations in monomer concentration on the elongation rate at two temperatures. At the highest temperature studied in this experiment (50℃), we find that a linear fit to the data does not intersect the concentration axis at 0, but at approximately 1.5 $\mu$M, corresponding to the equilibrium concentration, where growth and dissociation balance. At lower temperatures (illustrated at 10℃), the equilibrium concentration is too low to be resolvable by this method. This experiment provides an independent confirmation for the finding that for temperatures above approximately 45℃, the dissociation of the fibrils contributes significantly, and measurably, to the dynamics of the system.

In conclusion of this section, QCM is a powerful method for the resolution of small relative changes in fibril elongation rates, allowing both the temperature and concentration dependence of the fibril growth rate to be defined. However, the need to estimate both the mass sensitivity, as well as the surface fibril density of the QCM sensor in order to define absolute rates and rate constants illustrates that QCM is not an ideal method for these purposes. We therefore explored a in-solution alternative for quantifying the temperature-dependent

balance between fibril growth and dissociation.

*Solution based measurements of amyloid fibril growth and dissociation by differential scanning fluorimetry (DSF)*

If the rate of consumption of monomer can be directly quantified in solution, and the length distribution of the seed fibrils can be determined by imaging analysis, then the rate constants of fibril growth and dissociation can be defined more reliably than from surface-based biosensing [37]. The most convenient and least invasive way to perform such experiments is spectroscopically, either based on the fluorescence of an extrinsic label, such as Thioflavin-T (ThT) [38], or based on intrinsic protein fluorescence. We have shown recently that the change in tryptophan (Trp) emission spectrum is very pronounced upon conversion of the monomeric PI3K-SH3 into the fibrillar state [17]. The Trp emission is significantly quenched in the fibrillar state, probably due to ordered stacking of the Trp residues in the fibrils [39]. In the context of chemical denaturation studies, we have shown that intrinsic Trp fluorescence of PI3K-SH3 can be used to quantify the relative populations of monomer and fibrils as a function of chemical denaturant, without need for an extrinsic label, and we have determined the thermodynamic stability of the fibrils from equilibrium depolymerization experiments [15, 16, 17]. Here we explore capillary-based intrinsic fluorescence experiments in the form of differential scanning fluorimetry (DSF), a technique which allows to subject small volumes (approx. 10 $\mu$l) of samples to well-defined temperature profiles, such as temperature-jumps (T-jumps) and temperature ramps (T-ramps) with different scan rates while simultaneously monitoring the fluorescence emission intensity at 330 and 350 nm upon excitation at 280 nm.

We first tested whether the heat-induced dissociation of PI3K-SH3 amyloid fibrils could be followed by intrinsic Trp fluorescence (Figure 2 a) by heating the fibrils to 110°C in a differential scanning fluorimeter (see methods section for details). We found that the spectroscopic signature of fibrils (100 $\mu$M) subjected to such high temperatures converges towards the spectroscopic signature of monomeric protein at around 90°C, and upon cooling down does not convert

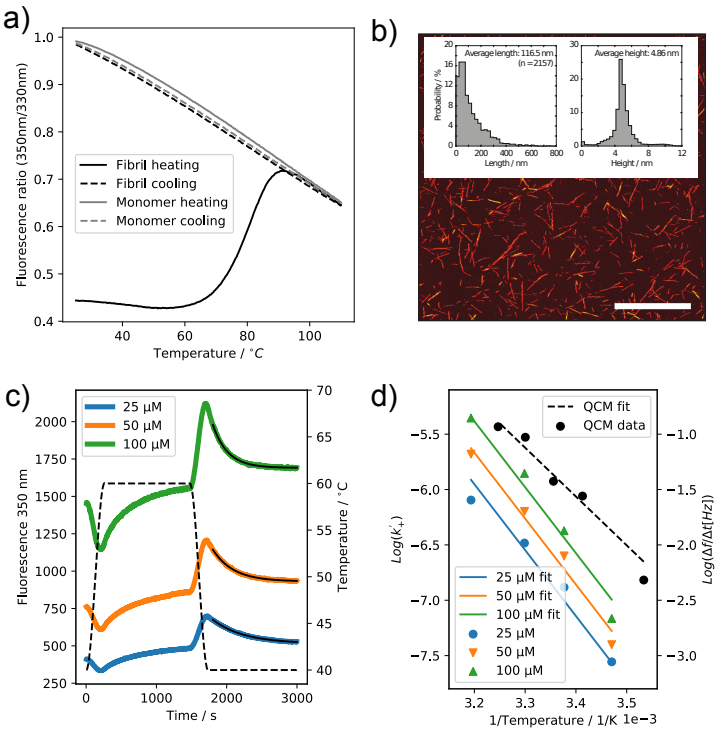


Figure 2: a) Full thermal denaturation of 100 $\mu$M PI3K-SH3 amyloid fibrils, with a monomer sample at the same concentration as control. The down scans shows that the protein had become fully monomeric at temperatures above approximately 90°C. The inset shows full emission spectra in the relevant wavelength region of PI3K-SH3 fibrils before and after thermal treatment of 10 minutes at 90°C. b) AFM image of sonicated PI3K-SH3 amyloid fibrils. Length and thickness distributions as determined from automated image analysis are shown as insets. Scale bar indicates 1 $\mu$M. c) Fibril dissociation at 60°C for 20 minutes is followed by a rapid change to 40°C, and the re-growth of the fibrils is monitored. d) Arrhenius-plots of the growth rate constants of the fibrils determined from experiments such as the one shown in c), where the lower temperature was varied. An Arrhenius-relationship was fitted to the data of the three different fibril concentrations by imposing a constant slope. For comparison, the Arrhenius-plot of the growth rates determined from QCM experiments is also shown.

back to its initial state, but behaves identical to the initially monomeric sample. This result confirms that PI3K-SH3 fibrils can be fully converted into monomer upon heating to high temperatures. Next, we established the usefulness and reliability of the DSF methodology in the context of our thermodynamic study of amyloid fibrils by probing the temperature-dependence of the fibril elongation rate through temperature-jump experiments. All the subsequent experiments were performed with sonicated fibrils, which has the advantage that higher order assembly/clumping of the fibrils is reduced, the length distribution is easier to determine and the kinetics is accelerated, due to the higher number of fibril ends. We subjected the PI3K-SH3 fibrils to ultrasound treatment (see methods section) and determined the length distribution by automated analysis of AFM images [40] (Figure 2 b). We observed that the ultrasound treatment not only significantly shortened the fibrils, but in addition also appears to separate the individual filaments, as seen from the resulting height distributions. Based on our recently reported cryo-EM structure of these fibrils [39], we determined the double filament fibrils to have a mass-per-length of 40 kDa/nm. We therefore used 20 kDa/nm as mass-per-length of the single filaments, in order to convert the length distributions into particle concentrations. We equilibrated fibril samples at 40℃ over night, loaded them into capillaries and inserted these into the DSF instrument, which had been pre-equilibrated at 40℃, followed by an immediate increase to 60℃, where the fibrils were incubated for 20 min. This leads to a certain degree of dissociation, releasing monomeric protein from the fibril ends. We then subjected the fibrils to rapid temperature changes to different lower temperatures, ranging from 15-40℃ and monitored the fibril growth and monomer depletion at each of these temperatures through the change in fluorescence signature. In supplementary section 3 we develop the theoretical framework for the analysis of such T-jump experiments of amyloid fibril growth. Intuitively, one might expect that the system relaxes with a time constant that is a combination of the characteristic rate constants of the system, i.e. $k_+$ and $k_-$, as is often observed in temperature jump relaxation experiments. However, we find that in the specific case of amyloid fibril elongation and dissociation, the

relaxation towards a new equilibrium state occurs always with the elongation rate constant, because only the rate of fibril elongation depends on the monomer concentration. We determined the elongation rate constants at the different temperatures from fits to exponential functions and performed Arrhenius-analysis, yielding an enthalpic barrier for fibril elongation of 49.5±3.1 kJ/mol, consistent with the result from the QCM experiments in this study, as well as previous reports [30]. This agreement establishes the validity of the DSF methodology for the study of amyloid fibril growth and dissociation. It is interesting to note that with the DSF method presented here, it is possible to determine the effective rate constant, $k'_+$ directly, whereas QCM measurements only yield rates. In appendix 4 we discuss in more detail the difference between Arrhenius-analysis on rates and rate constants. In order to determine the rate constant $k_+$, from $k'_+$, we need the concentration of growing fibril ends, [P]. We can determine [P] from the mass concentration of fibrils [M], together with the length distribution (from AFM image analysis) and mass per length (from the cryo-EM structure [39]). For [M] = 100 $\mu$M, we obtain [P] = 0.8 $\mu$M. From the measurements at three different values of [M] (25, 50 and 100 $\mu$M) at 23℃, we obtain an average value of $k_+ = 3500 \pm 1400$ $M^{-1}s^{-1}$. This value is in good agreement with the value that we have previously reported from QCM experiments [30] (2000 $M^{-1}s^{-1}$), under conditions where the QCM sensor was less crowded and where a better estimation of the mass sensitivity and surface fibril concentration could be achieved compared to the very highly crowded conditions of the present study.

We then performed another series of temperature jump experiments, starting with fibrils equilibrated at 40℃. This time we varied the upper temperature (60-75℃) and monitored the relaxation of the system, which occurs through a net dissociation of fibrillar mass (Figure 3 a). Interestingly, our mathematical analysis shows that even in this case, the exponential relaxation constant corresponds solely to the rate constant of fibril elongation. All information about the dissociation rate constant is contained in the amplitude of the relaxation or, equivalently, the slope of a linear approximation of the initial part of the relaxation phase (see supplementary section 3).

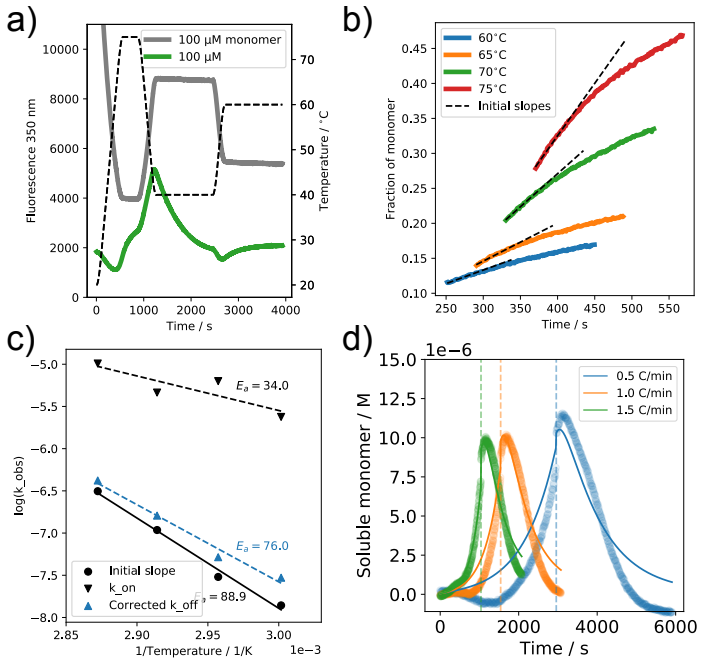


Figure 3: a) Temperature variation scheme including a brief period at 75°C, followed by equilibration at 40°C and a rapid temperature change to 60°C, where the dissociation is monitored. b) The dissociation phases upon increase in temperature to 60, 65, 70 and 75°C. The interrupted lines illustrate the fits to the initial slopes. c) Arrhenius-plots for the growth rate constant (from the exponential relaxation to the new equilibrium at high temperature), as well as for the dissociation rate constants (from initial slopes as well as with correction factor, see supplementary section 3). d) Temperature ramp of 25 $\mu$M fibrils at three different scan rates (0.5, 1 and 1.5°C/min), including a global fit with fixed $\Delta H_+^{\ddagger}$, as well as the constraint that $\frac{k_-(50°C)}{k_+(50°C)} = 1.5$ $\mu$M (see supplementary section 6).

We verified this theoretical result by performing Arrhenius-analysis for both the exponential constants as well as for the initial slopes (Figure 3 b and c) and we find that the two Arrhenius-plots have very different slopes. The Arrhenius-analysis of the exponential constants yields an activation energy (34.0±14.3 kJ/mol) slightly lower than what we found for the elongation rate constant at lower temperatures, possibly indicating a non-negligible temperature dependence/heat capacity of the transition state for fibril elongation, see section above. The difference of approximately 15 kJ/mol over a temperature range of ca. 40℃ suggests a $\Delta C_p$ of the order of 0.4 kJ/(mol·K). This value is lower than the one obtained from the global fit of the temperature dependence at different concentrations measured by QCM (1.3 kJ/(mol·K) see supplementary figure 1); however, both methods consistently require the inclusion of a temperature dependent energy barrier for the fibril growth reaction. The Arrhenius-analysis of the initial slopes, on the other hand, yields a significantly higher activation enthalpy ($\Delta H^{\ddagger}$ = 88.9 kJ/mol±7.3 kJ/mol), which is in good agreement with the estimate of the enthalpic barrier for fibril dissociation estimated from the QCM experiments (see above). In supplementary section 3 we discuss how we correct the Arrhenius-plot extracted from the initial slopes to obtain an improved approximation of the temperature dependence of the dissociation rate constants. This correction leads to a small decrease in the slope of the Arrhenius-plot. However, it can clearly be seen from Figure 3 b) that the initial slopes for the experiments at different upper temperatures are measured at different time points after the temperature jump is induced. This is caused by the finite time required to reach the different upper temperatures, and leads possibly to an underestimation of the temperature dependence of fibril dissociation. We finally explored the applicability of an additional feature of the DSF instrument, namely the possibility to subject the amyloid fibrils to continuous temperature ramps at constant and well-defined slope. Figure 3 d) shows data from an experiment, where 100 $\mu$M of fibrils are subjected to temperature ramps from 40-65℃ and back to 40℃ at three different ramping speeds (0.5, 1.0 and 1.5 ℃/min). In these experiments, we use the fibril and monomer references in order to convert

the spectroscopic signal into an absolute monomer concentration. We find that the highest monomer concentration is reached while the fibrils are already cooling down, suggesting that the rate of temperature change is in all cases too fast for the system to be able to equilibrate at all temperatures. When the fibrils reach the maximal temperature, the monomer concentration is still below the equilibrium concentration, and the fibrils continue to dissociate while the fibrils are cooled down, up to the point where the monomer concentration coincides with the equilibrium concentration at the specific temperature. Further cooling then reverts the situation, i.e. the monomer concentration is then higher than the equilibrium concentration and the the fibrils will start to grow again. The faster the scan rate the larger the deviation between equilibrium concentration and actual concentration at the highest temperature reached and hence the more asymmetric the overall time course of monomer concentration. We fitted a model to the temperature ramp data, where we fixed the temperature dependence of the elongation rate constant to the range of values determined from the QCM and temperature jump experiments. Furthermore, we added the additional constraint that the ratio of the dissociation and growth rate constants, i.e. the critical concentration, at 50℃ is equal to that determined from our QCM experiments (supplementary figure 2). Details of the model and how the fit result of the activation enthalpy for the dissociation reaction depend on the magnitude of the activation enthalpy for the elongation reaction, as well as on the imposed constraint can be found in supplementary section 6. For $\Delta H_+^\ddagger$ = 40 kJ/mol and $c_{crit}$ = 1.5 $\mu$M, we obtain $\Delta H_-^\ddagger \approx$ 167 kJ/mol. This value is significantly larger than the estimate from the temperature jumps, but we find that it depends very sensitively on the imposed constraint, i.e. the exact value of the equilibrium monomer concentration at a reference temperature (here 50℃) that we impose (see supplementary section 6). A change from 1.5 to 3 $\mu$M changes the value of $\Delta H_-^\ddagger$ from >160 kJ/mol to <120 kJ/mol. Despite these uncertainties, we can use the results of the fit to the temperature ramp to extrapolate the ratio of dissociation and growth rate constant to lower temperatures and hence estimate the thermodynamic stability of the fibrils at

temperatures outside the temperature range used in the ramping experiments. This analysis leads to $c_{eq} = 0.046$ $\mu$M at 28℃, a value approximately 10 times lower than the one from the QCM experiments, corresponding to a free energy difference of -42.2 kJ/mol for the fibrillar state with respect to the monomeric state.

## Discussion

At physiological temperature ranges and below, most amyloid fibrils are found to be so stable that the equilibrium concentration of monomer is too low to be reliably quantified. A notable exception to this rule are the fibrils of the protein $\alpha$-synuclein, which have been shown to be able to undergo cold denaturation, i.e. dissociation at temperatures close to the freezing point of water [41, 18]. On the other hand, while many amyloid fibrils are known to be heat sensitive, the fibrils are often only found to fully dissolve at temperatures above 100℃ [42, 43]. Here we investigate the thermodynamic stability of PI3K-SH3 amyloid fibrils through measurements of fibril growth and dissociation at different temperatures, using both surface-based biosensing, as well as solution-based temperature perturbation methods based on intrinsic protein fluorescence. We find that both types of measurements agree overall in that at temperatures below 45℃, the dissociation rate is too slow to be resolved, but that it increases rapidly at higher temperatures due to a significantly greater temperature dependence compared to that of the growth rate constant (activation enthalpies >100 kJ/mol vs <50 kJ/mol). The latter shows decrease in magnitude with increasing temperature. The balance between fibril growth and dissociation does not only depend on temperature, but also on the concentration of monomeric protein, because only the growth rate depends on soluble protein concentration. This concentration dependence explains why we did not detect the strong increase in dissociation rate with temperature in a previous study, where we performed QCM experiments with 100 $\mu$M of protein [30], whereas in the present study we performed the initial experiments at the much lower

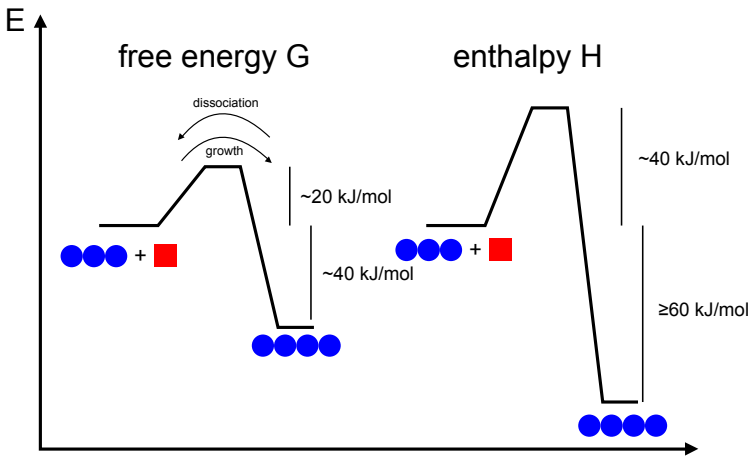


Figure 4: Energy landscapes of PI3K-SH3 amyloid fibril growth around room temperature. Left: free energy landscape, right: energy/enthalpy landscape.

concentration of 5 $\mu$M, as well as over a wider temperature range up to 60°C.

From the direct comparison of two label-free experimental techniques, one surface-based (QCM) and one solution based (DSF), we conclude that while QCM is able to resolve small relative changes in fibril elongation rate, estimates of absolute rates are associated with significant uncertainties, due to the necessity to estimate both the mass sensitivity, as well as the surface concentration of the fibrils. These estimates present particular challenges when the surface density of fibrils is maximised, as was the case in the present study. Solution based methods, on the other hand, require an accurate determination of the fibril length distribution, in order to define the concentration of growth competent ends [38, 37]. Reliable and accurate methods for this purpose have been developed [40] and allow us to provide a robust estimate for the fibril end concentration and therefore the absolute rate constants. The rate constants, in turn, allow us to calculate the thermodynamic stability of the fibrils in the form of an association equilibrium constant of a monomer interacting with a fibril end, according to $K = m_{eq} = \frac{k_-}{k_+}$. An interesting aspect to consider is to compare

the thermodynamic stability of the fibrils obtained from the kinetic experiments in this paper with that obtained through equilibrium depolymerisation. Here we find thermodynamic stabilities of 36.2 kJ/mol (from QCM) and 42.3 kJ/mol (DSF) at 28℃, whereas in our recent chemical depolymerization experiments of PI3K-SH3 amyloid fibrils with urea [17], we reported a value of approximately 60 kJ/mol, determined from fits of the chemical depolymerization with the cooperative linear polymerization model. These measurements were performed under different solution conditions. The kinetic experiments of the present studywere performed in 10 mM glycine-HCL buffer, which has an ionic strength of approximately 6 mM, because the Zwitterionic form of the buffer does not contribute to the solution ionic strength [44]. The chemical depolymerization experiments with urea, on the other hand, were performed in an ionic strength range of 27 to 47 mM. If we extrapolate the ionic strength dependence back into the regime where the kinetic experiments were performed, using the slope at the lower ionic strength end of the chemical depolymerization, we obtain a predicted stability of 41 kJ/mol, in excellent agreement with the measured values in the present study. This result underlines that amyloid fibril elongation indeed behaves like a well-defined two state system, the thermodynamics of which can be reliably determined from both equilibrium and non-equilibrium experiments. However, the different solution conditions utilised in these two types of experiment render a direct comparison non-trivial, due to the very strong ionic strength dependence of amyloid fibril stability, in particular for fibrils formed under low pH conditions, where the monomeric building blocks carry a large net charge [17]. Such a comparison will therefore be even more challenging if ionic denaturants, such as GnDHCl are used [15, 16, 22]. In the present study we are able to resolve the contribution of the dissociation rate at elevated temperatures because the stability of the fibrils is reduced at very low ionic strength. In a previous study based on H/D-exchange, it has been found that at low ionic strength (10 mM), monomer recycling of PI3K-SH3 fibrils is so rapid, that on a time scale of several days, up to half of the monomer in fibrils is exchanged at 28℃ [45]. The values of the growth and dissociation rate constants reported

in [45] ($k_+$=1.4$M^{-1}s^{-1}$ and $k_-$=7.1·$10^{-5}s^{-1}$) predict an equilibrium monomer concentration of 50 $\mu$M at 28℃. Here we find from direct measurements that this concentration is ca. 1.5 $\mu$M at 50℃ and from the extrapolated values of the rate constants at 28℃ ($k_+$ = 3500 $M^{-1}s^{-1}$ (T-jump) and 1000 $M^{-1}s^{-1}$ (T-ramp); $k_-$ = 4.7·$10^{-5}s^{-1}$) we obtain an equilibrium monomer concentration of the order of tens of nM. Our value for $k_-$ is very similar to that from [45], but our value for $k_+$ is approximately 3 orders of magnitude larger. The fact that our estimate stems from several independent and direct measurements, as well as its close agreement with an earlier estimate [30] renders our estimate very robust. These findings highlight the value of direct measurements of the molecular rate constants and/or the equilibrium monomer concentration if it is high enough [22] as opposed to through indirect measurements, such as from isotope exchange experiments [45]. However, as we outline in supplementary section 5, the simple relationship between soluble protein concentration and thermodynamic stability is only valid if the total protein concentration is much larger than the soluble concentration. This requirements puts limits on the regime in which the stability can be easily determined from a measurement of the soluble protein concentration. The present study is among the first to also quantify the temperature dependence of the fibril dissociation reaction. We are only aware of one other study [46], where a quantitative analysis of fibril (amyloid $\beta$ protofilaments) dissociation is performed at different temperatures, yielding a larger enthalpy of activation of dissociation (80 kJ/mol) than the enthalpy of activation determined for (mature) fibril growth (66 kJ/mol) [30]. Here we obtain three different estimates of the enthalpy of activation of fibril dissociation, from QCM (ca. 105 kJ/mol), from T-jump (ca. 80-90 kJ/mol) and from T-ramp (ca. 170 kJ/mol). The value determined from T-jump represents a lower bound, whereas the value from the T-ramp shows a strong dependence on the imposed constraints and is likely to represent an upper bound. We conclude that the enthalpy barrier for fibril dissociation is of the order of 100 kJ/mol or higher. From our study emerges a picture of the free energy and enthalpy landscape of the elongation reaction of PI3K-SH3 fibrils illustrated in Figure 4. Both

the enthalpic barriers and stabilities are higher than the equivalent free energies, which illustrates the typical enthalpy entropy compensation found in many biomolecular reactions [47]. The enthalpic interactions to be broken to enable the transition from the fibrillar to the monomeric state are found to be significantly larger than those to reach the fibrillar state from the monomeric one, probably reflecting the higher degree of secondary structure in the fibrillar state compared to the monomer at pH 2 [5]. The same qualitative behaviour is also found for the amyloid $\beta$-peptide [46] which forms fibrils at neutral pH. These results from non-equilibrium experiments of growth and dissociation, namely that amyloid fibril formation is enthalpically favourable (Figure 4) are in excellent agreement with comprehensive calorimetric experiments of amyloid fibril growth that show that amyloid fibril growth is in general exothermic at moderate to higher temperatures [18]. In the calorimetric experiments, it was found that amyloid fibril growth had in most cases a significant negative heat capacity. This implies that the growth reaction becomes more enthalpically favourable at higher temperatures, which could stem from the reactants becoming enthalpically less favourable (possibly leading to a decrease in barrier height for growth) or the products becoming more favourable (possibly leading to an increase in barrier height for dissociation). From the T-jump experiments in the different temperature ranges, we have evidence that the activation enthalpy of the elongation rate constant decreases at higher temperatures and also the QCM experiments require an activation heat capacity to be quantitatively fittable. We did not find it necessary in our modeling to also include a temperature dependent enthalpy of activation for dissociation, but it can be argued that it is a somewhat arbitrary choice to allow only the energy barrier for fibril growth to depend on temperature. However, the fact that we can consistently describe the thermodynamics of the PI3K-SH3 amyloid fibril system over a wide temperature range even without taking activation heat capacities into account suggests that temperature dependencies of the activation enthalpies of both growth and dissociation are probably small.

## Conclusions

In conclusion, we have measured the temperature dependencies of the growth and dissociation rates of PI3K-SH3 amyloid fibrils by both established surface-based biosensing measurements and novel solution based differential scanning fluorimetry. We find that the dissociation rate displays a much stronger temperature dependence than the growth rate, which leads to the fact that the solubility of the protein rises steeply above 50℃. In addition to this fundamental result on the physical chemistry of amyloid assembly, we establish temperature perturbation (T-jump and T-ramp) experiments as a novel strategy to probe the thermodynamics of amyloid fibrils, with the potential to be applied at high throughput. A detailed understanding of the origins and magnitude of the thermodynamic stability of disease-related amyloid fibrils, which can be achieved with the methods developed and applied here to a model amyloid system, will enable to better rationalise the fate and persistence of amyloid fibrils in diseased individuals.

## Acknowledgements

AKB and RKN thank the Novo Nordisk Foundation for funding (NNFSA170028392). AKB and NV thank the Deutsche Forschungsgemeinschaft (DFG) for funding. AC acknowledges support through an Erasmus+ traineeship. WFX is supported by funding from the Biotechnology and Biological Sciences Research Council (BBSRC), UK grant BB/S003312/1. The authors thank Thomas C.T. Michaels for helpful discussions.

## References

[1] R. P. McGlinchey, F. Shewmaker, P. McPhie, B. Monterroso, K. Thurber, R. B. Wickner, The repeat domain of the melanosome fibril protein pmel17 forms the amyloid core promoting melanin synthesis., Proc Natl Acad Sci U S A 106 (33) (2009) 13731–13736. doi:10.1073/pnas.0906509106. URL http://dx.doi.org/10.1073/pnas.0906509106

[2] S. K. Maji, M. H. Perrin, M. R. Sawaya, S. Jessberger, K. Vadodaria, R. A. Rissman, P. S. Singru, K. P. R. Nilsson, R. Simon, D. Schubert, D. Eisenberg, J. Rivier, P. Sawchenko, W. Vale, R. Riek, Functional amyloids as natural storage of peptide hormones in pituitary secretory granules, Science 325 (2009) 328–332.

[3] M. Andreasen, G. Meisl, J. D. Taylor, T. C. Michaels, A. Levin, D. E. Otzen, M. R. Chapman, C. M. Dobson, S. J. Matthews, T. P. Knowles, Physical determinants of amyloid assembly in biofilm formation, Mbio 10 (1) (2019) e02279–18.

[4] S. Koyama, H. Yu, D. C. Dalgarno, T. B. Shin, L. D. Zydowsky, S. L. Schreiber, Structure of the pi3k sh3 domain and analysis of the sh3 family., Cell 72 (6) (1993) 945–952.

[5] J. Zurdo, J. I. Guijarro, J. L. Jimenez, H. R. Saibil, C. M. Dobson, Dependence on solution conditions of aggregation and amyloid formation by an SH3 domain., J Mol Biol 311 (2) (2001) 325–340. doi:10.1006/jmbi.2001.4858.
URL http://dx.doi.org/10.1006/jmbi.2001.4858

[6] J. I. Guijarro, C. J. Morton, K. W. Plaxco, I. D. Campbell, C. M. Dobson, Folding kinetics of the sh3 domain of pi3 kinase by real-time nmr combined with optical spectroscopy., Journal of molecular biology 276 (1998) 657–667. doi:10.1006/jmbi.1997.1553.

[7] J. I. Guijarro, M. Sunde, J. A. Jones, I. D. Campbell, C. M. Dobson, Amyloid fibril formation by an SH3 domain., Proc Natl Acad Sci U S A 95 (8) (1998) 4224–4228.

[8] M. Bucciantini, E. Giannoni, F. Chiti, F. Baroni, L. Formigli, J. Zurdo, N. Taddei, G. Ramponi, C. M. Dobson, M. Stefani, Inherent toxicity of aggregates implies a common mechanism for protein misfolding diseases., Nature 416 (6880) (2002) 507–511. doi:10.1038/416507a.
URL http://dx.doi.org/10.1038/416507a

[9] A. Orte, N. R. Birkett, R. W. Clarke, G. L. Devlin, C. M. Dobson, D. Klenerman, Direct characterization of amyloidogenic oligomers by single-molecule fluorescence., Proc Natl Acad Sci U S A 105 (38) (2008) 14424–14429. doi:10.1073/pnas.0803086105.
URL http://dx.doi.org/10.1073/pnas.0803086105

[10] J. L. Jimenez, J. I. Guijarro, E. Orlova, J. Zurdo, C. M. Dobson, M. Sunde, H. R. Saibil, Cryo-electron microscopy structure of an SH3 amyloid fibril and model of the molecular packing., EMBO J 18 (4) (1999) 815–821. doi:10.1093/emboj/18.4.815.
URL http://dx.doi.org/10.1093/emboj/18.4.815

[11] P. P. de Laureto, N. Taddei, E. Frare, C. Capanni, S. Costantini, J. Zurdo, F. Chiti, C. M. Dobson, A. Fontana, Protein aggregation and amyloid fibril formation by an SH3 domain probed by limited proteolysis., J Mol Biol 334 (1) (2003) 129–141.

[12] M. J. Bayro, T. Maly, N. R. Birkett, C. E. Macphee, C. M. Dobson, R. G. Griffin, High-resolution mas nmr analysis of pi3-sh3 amyloid fibrils: backbone conformation and implications for protofilament assembly and structure ., Biochemistry 49 (35) (2010) 7474–7484. doi:10.1021/bi100864t.
URL http://dx.doi.org/10.1021/bi100864t

[13] C. M. Dobson, Protein folding and misfolding., Nature 426 (6968) (2003) 884–890. doi:10.1038/nature02261.
URL http://dx.doi.org/10.1038/nature02261

[14] C. M. Dobson, The amyloid phenomenon and its links with human disease., Cold Spring Harbor perspectives in biology (Jan 2017). doi:10.1101/cshperspect.a023648.

[15] T. Narimoto, K. Sakurai, A. Okamoto, E. Chatani, M. Hoshino, K. Hasegawa, H. Naiki, Y. Goto, Conformational stability of amyloid fibrils of beta2-microglobulin probed by guanidine-hydrochloride-induced unfolding., FEBS Lett 576 (3) (2004) 313–319. doi:10.1016/j.febslet.2004.

09.024.
URL http://dx.doi.org/10.1016/j.febslet.2004.09.024

[16] A. J. Baldwin, T. P. J. Knowles, G. G. Tartaglia, A. W. Fitzpatrick, G. L. Devlin, S. L. Shammas, C. A. Waudby, M. F. Mossuto, S. Meehan, S. L. Gras, J. Christodoulou, S. J. Anthony-Cahill, P. D. Barker, M. Vendruscolo, C. M. Dobson, Metastability of native proteins and the phenomenon of amyloid formation., J Am Chem Soc 133 (36) (2011) 14160–14163. doi:10.1021/ja2017703.
URL http://dx.doi.org/10.1021/ja2017703

[17] N. Vettore, A. K. Buell, Thermodynamics of amyloid fibril formation from chemical depolymerization, Physical Chemistry Chemical Physics 21 (47) (2019) 26184–26194.

[18] J. H. M. van Gils, E. van Dijk, A. Peduzzo, A. Hofmann, N. Vettore, M. P. Schützmann, G. Groth, H. Mouhib, D. E. Otzen, A. K. Buell, et al., The hydrophobic effect characterises the thermodynamic signature of amyloid fibril growth, PLOS Computational Biology 16 (5) (2020) e1007767.

[19] J. Dubois, A. ISMAIL, S. CHAN, Z. Ali-Khan, Fourier transform infrared spectroscopic investigation of temperature-and pressure-induced disaggregation of amyloid a, Scandinavian journal of immunology 49 (4) (1999) 376–380.

[20] K. Sasahara, H. Naiki, Y. Goto, Kinetically controlled thermal response of beta2-microglobulin amyloid fibrils., J Mol Biol 352 (3) (2005) 700–711. doi:10.1016/j.jmb.2005.07.033.
URL http://dx.doi.org/10.1016/j.jmb.2005.07.033

[21] B. Morel, L. Varela, F. Conejero-Lara, The thermodynamic stability of amyloid fibrils studied by differential scanning calorimetry., J Phys Chem B 114 (11) (2010) 4010–4019. doi:10.1021/jp9102993.
URL http://dx.doi.org/10.1021/jp9102993

[22] J. Kardos, A. Micsonai, H. Pál-Gábor, É. Petrik, L. Gráf, J. Kovács, Y.-H. Lee, H. Naiki, Y. Goto, Reversible heat-induced dissociation of $\beta$2-microglobulin amyloid fibrils, Biochemistry 50 (15) (2011) 3211–3220.

[23] T. Kawasaki, J. Fujioka, T. Imai, K. Torigoe, K. Tsukiyama, Mid-infrared free-electron laser tuned to the amide i band for converting insoluble amyloid-like protein fibrils into the soluble monomeric form, Lasers in medical science 29 (5) (2014) 1701–1707.

[24] N. T. Co, P. D. Lan, P. D. Q. Huy, M. S. Li, Heat-induced degradation of fibrils: Exponential vs logistic kinetics, J. Chem. Phys. 152 (2020) 115101.

[25] B. O'Nuallain, S. Shivaprasad, I. Kheterpal, R. Wetzel, Thermodynamics of a beta(1-40) amyloid fibril elongation., Biochemistry 44 (38) (2005) 12709–12718. doi:10.1021/bi050927h.
URL http://dx.doi.org/10.1021/bi050927h

[26] A. D. Williams, S. Shivaprasad, R. Wetzel, Alanine scanning mutagenesis of abeta(1-40) amyloid fibril stability., Journal of molecular biology 357 (2006) 1283–1294. doi:10.1016/j.jmb.2006.01.041.

[27] K. Brännström, A. Öhman, L. Nilsson, M. Pihl, L. Sandblad, A. Olofsson, The n-terminal region of amyloid $\beta$ controls the aggregation rate and fibril stability at low ph through a gain of function mechanism., Journal of the American Chemical Society 136 (2014) 10956–10964. doi:10.1021/ja503535m.

[28] M. Eigen, G. G. Hammes, Kinetic studies of adp reactions with the temperature jump method, J Am Chem Soc 82 (22) (1960) 5951–5952.

[29] A. K. Buell, D. A. White, C. Meier, M. E. Welland, T. P. J. Knowles, C. M. Dobson, Surface attachment of protein fibrils via covalent modification strategies., J Phys Chem B 114 (34) (2010) 10925–10938. doi:10.1021/jp101579n.
URL http://dx.doi.org/10.1021/jp101579n

[30] A. K. Buell, A. Dhulesia, D. A. White, T. P. J. Knowles, C. M. Dobson, M. E. Welland, Detailed analysis of the energy barriers for amyloid fibril growth., Angew Chem Int Ed Engl 51 (21) (2012) 5247–5251. doi:10.1002/anie.201108040.
URL http://dx.doi.org/10.1002/anie.201108040

[31] J. D. Bryngelson, J. N. Onuchic, N. D. Socci, P. G. Wolynes, Funnels, pathways, and the energy landscape of protein folding: a synthesis., Proteins 21 (3) (1995) 167–195.

[32] T. Schindler, F. X. Schmid, Thermodynamic properties of an extremely rapid protein folding reaction, Biochemistry 35 (1996) 16833–16842.

[33] Y.-J. Tan, M. Oliveberg, A. R. Fersht, Titration properties and thermodynamics of the transition state for folding: comparison of two-state and multi-state folding pathways, Journal of molecular biology 264 (2) (1996) 377–389.

[34] M. L. Scalley, D. Baker, Protein folding kinetics exhibit an Arrhenius temperature dependence when corrected for the temperature dependence of protein stability., Proc Natl Acad Sci U S A 94 (20) (1997) 10636–10640.

[35] T. P. J. Knowles, W. Shu, G. L. Devlin, S. Meehan, S. Auer, C. M. Dobson, M. E. Welland, Kinetics and thermodynamics of amyloid formation from direct measurements of fluctuations in fibril mass., Proc Natl Acad Sci U S A 104 (24) (2007) 10016–10021. doi:10.1073/pnas.0610659104.
URL http://dx.doi.org/10.1073/pnas.0610659104

[36] A. K. Buell, C. M. Dobson, M. E. Welland, Amyloid Proteins - Methods and Protocols, 2nd Edition, Vol. 849 of Methods in Molecular Biology, Humana Press, 2012.

[37] A. K. Buell, The growth of amyloid fibrils: rates and mechanisms, Biochemical Journal 476 (19) (2019) 2677–2703.

[38] A. K. Buell, C. Galvagnion, R. Gaspar, E. Sparr, M. Vendruscolo, T. P. J. Knowles, S. Linse, C. M. Dobson, Solution conditions determine the relative importance of nucleation and growth processes in $\alpha$-synuclein aggregation., Proc Natl Acad Sci U S A 111(21) (2014) 7671–7676. doi:10.1073/pnas.1315346111.
URL http://dx.doi.org/10.1073/pnas.1315346111

[39] C. Röder, N. Vettore, L. N. Mangels, L. Gremer, R. B. Ravelli, D. Willbold, W. Hoyer, A. K. Buell, G. F. Schröder, Atomic structure of pi3-kinase sh3 amyloid fibrils by cryo-electron microscopy, Nature Communications 10 (2019) 3754.

[40] W.-F. Xue, S. W. Homans, S. E. Radford, Amyloid fibril length distribution quantified by atomic force microscopy single-particle image analysis, Protein Engineering, Design & Selection 22 (8) (2009) 489–496.

[41] T. Ikenoue, Y.-H. Lee, J. Kardos, M. Saiki, H. Yagi, Y. Kawata, Y. Goto, Cold denaturation of alpha-synuclein amyloid fibrils., Angew Chem Int Ed Engl (Jun 2014). doi:10.1002/anie.201403815.
URL http://dx.doi.org/10.1002/anie.201403815

[42] A. Arora, C. Ha, C. B. Park, Insulin amyloid fibrillation at above 100 degrees c: new insights into protein folding under extreme temperatures., Protein Sci 13 (9) (2004) 2429–2436. doi:10.1110/ps.04823504.
URL http://dx.doi.org/10.1110/ps.04823504

[43] U. Baxa, P. D. Ross, R. B. Wickner, A. C. Steven, The n-terminal prion domain of ure2p converts from an unfolded to a thermally resistant conformation upon filament formation, Journal of molecular biology 339 (2) (2004) 259–264.

[44] E. Stellwagen, J. D. Prantner, N. C. Stellwagen, Do zwitterions contribute to the ionic strength of a solution?, Analytical biochemistry 373 (2) (2008) 407–409.

# Supplementary materials: Thermodynamics of amyloid fibril growth from non-equilibrium experiments of growth and dissociation

Rasmus K. Norrild*

*Technical University of Denmark, Department of Biotechnology and Biomedicine*

Nicola Vettore*

*Technical University of Denmark, Department of Biotechnology and Biomedicine*

Alberto Coden*

*Technical University of Denmark, Department of Biotechnology and Biomedicine*

Wei-Feng Xue

*School of Biosciences, University of Kent*

Alexander K. Buell[1]

*Technical University of Denmark, Department of Biotechnology and Biomedicine*

**These authors contributed equally to the work*

## 1. Supplementary data

Supplementary figure 1 shows the result of an experiment where the temperature-dependence of the fibril elongation rate was measured at three different monomer concentrations. It can clearly be seen that degree of curvature observed at higher temperatures depends on the monomer concentration. We globally fitted the data set to a model with temperature independent activation energies. The fit yields the following results: $\Delta H_+^{\ddagger}$ 40.5±1.6, $\Delta H_-^{\ddagger}$ = 75.4±27.1). If we include a heat capacity change, i.e. a temperature dependence of the activation energy/enthalpy of the elongation reaction $\Delta C_p$, we obtain the following results: ($\Delta C_p$ = 1.3 kJ/mol/K, $\Delta H_-^{\ddagger}$ = 67.5±22.7 kJ/mol). While a global fit to a

[1]to whom correspondence should be addressed: alebu@dtu.dk

larger data set represents in general a more stringent test of our model than the fit to a single concentration in Figure 1, a significant difficulty stems from the fact that such an extended data set cannot be acquired with a single QCM sensor. The finite number of data points that can be extracted from each sensor before the fibrils are too long to be reliably detected requires combining data sets from different sensors, which involves normalisation based on a reference condition (see methods section).

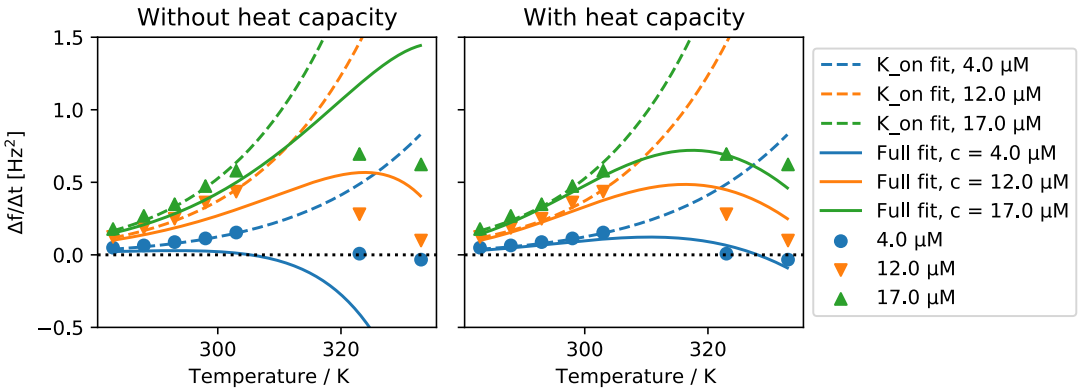


Figure 1: Global Fitting of temperature-dependent QCM data of PI3K-SH3 amyloid fibrils at three concentrations of monomer. Left: global fit with temperature independent activation energies for growth and dissociation. Right: Global fit with inclusion of a heat capacity for the activation energy of fibril growth.

We also measured the concentration-dependence of the fibril elongation rate at low concentrations (1-5 $\mu$M) at two different temperatures (10℃ and 50℃). The results are shown in supplementary figure 2. We find that at 50℃, the best linear fit intercepts the x-axis at a concentration of approximately 1.5 $\mu$M. This concentration corresponds to the critical concentration of the elongation reaction at 50℃.

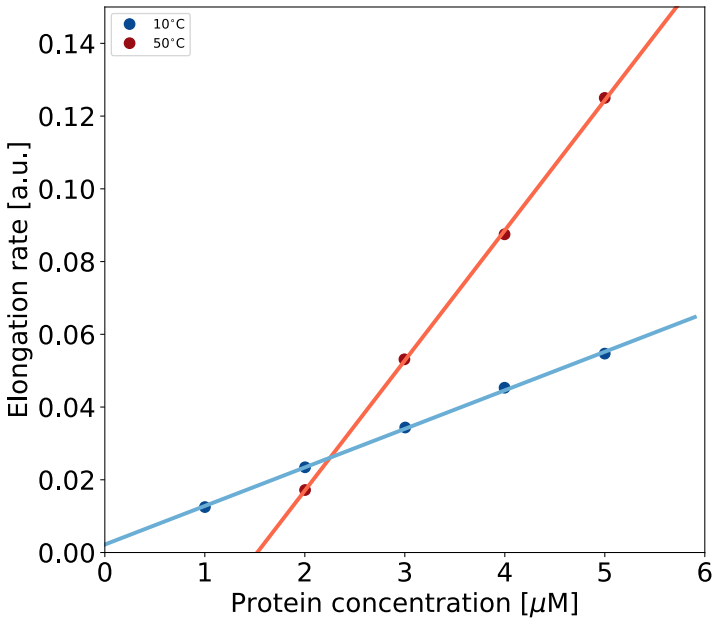


Figure 2: QCM experiment to probe the concentration-dependence of the fibril growth rate at 10°C and 50°C.

## 2. Analysis of QCM experiments

The rates of fibril elongation and dissociation using the QCM are initially obtained in the units of change of resonant frequency per unit time, $\frac{\Delta f}{\Delta t}$, with units of Hz/s, i.e. $s^{-2}$. In order to be able to fit a model that contains molecular rate constants to the QCM data at different temperatures and concentrations, the rate of change of frequency needs to be translated into the number of addition or dissociation events with respect to a single fibril end. This conversion involves a series of assumptions and estimates that introduce significant uncertainty. First of all, we require the mass sensitivity of the QCM for amyloid fibril growth. We have previously determined that the mass sensitivity of amyloid fibril growth is considerably higher than the Sauerbrey mass sensitivity of the crystals we used in our experiments (17.7 ng/Hz). This mass sensitivity is valid for rigid layers in vacuum or air. We have found an approximately 4-fold higher

mass sensitivity of the order of 4 ng/Hz[1]. This mass sensitivity was determined at 55℃. It is possible that the mass sensitivity depends on temperature as both the density (somewhat) and viscosity (strongly) of the solvent water depend on temperature. However, we neglect this dependence here as it is not precisely known and unlikely to much exceed the relative change in viscosity (ca. factor 2.5) throughout the temperature window of our experiments (15-65℃). Therefore, 1 Hz/s of frequency change translates into 4 ng of of dry protein mass attaching to the sensor every second. The molecular mass of the PI3K-SH3 monomer is 9500 Da, and hence 4 ng correspond to $2.5{\cdot}10^{11}$ molecules of PI3K-SH3 per second. We next need to estimate the surface density of growth competent ends. In previous work, we have estimated this number from analysis of AFM images [2]. However, in the present study we have maximised the surface density to an extent that renders it very difficult to provide even an approximate estimate (Supplementary Figure 3).

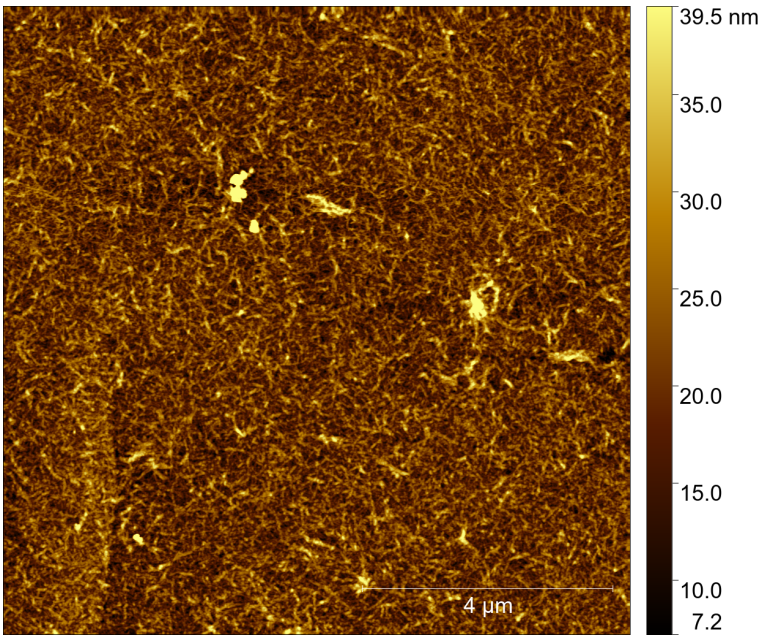


Figure 3: AFM image of a QCM sensor after an elongation experiment, illustrating the very high surface density of fibrils that form a multilayer on the sensor surface.

We therefore estimate the surface density from a direct comparison of the rates of frequency change between our previous [2] and present studies. Previously, we have observed a rate of approximately 1.5 Hz/min at a protein concentration of 100 $\mu$M and an estimated surface concentration of 100 fibrils per $\mu m^2$. Here we observe a rate that is approximately 10 times higher, at a 10 times lower concentration, suggesting that the fibril concentration could be up to a 100 fold higher. However, this leads to an unrealistically high estimate of 10000 fibrils per $\mu m^2$. It is more likely that upon increase of the surface-density, more solvation water is detected upon fibril growth, leading to the mass sensitivity becoming even higher. This discussion illustrates the large uncertainty associated with the definition of absolute amyloid fibril growth rates by QCM. This should be kept in mind when we proceed with a more realistic estimate of 1000 fibrils per $\mu m^2$, corresponding to a 10 fold higher surface density than in our previous study [2]. This estimate translates into $2{\cdot}10^{11}$ fibril ends per $cm^2$ of surface area. Taken together, we find that a rate of frequency change of 1 Hz/s corresponds to approximately 1 molecule of PI3K-SH3 per fibril end at 1 Hz/s. We use this conversion factor in our fits of the QCM data We therefore need to scale the raw data by this factor in order to work in molar units.

The second important point to consider is as to the kinetic pre-factor of the expressions of fibril growth and dissociation. We treat here the growth and dissociation separately.

### *2.1. Fibril growth*

The rate of growth of a population of fibrils is given by

$$\frac{dM}{dt} = k_+[P][m] \tag{1}$$

where [M] is the fibril mass concentration in monomer equivalents, [P] is the number concentration of fibril ends, [m] is the monomer concentration and $k_+$ is the elongation rate constant with units of $[(\mathrm{mol/l})^{-1}\ \mathrm{s}^{-1}]$. The growth rate per fibril end is given by:

$$\frac{dM}{[P]dt} = k_+[m] \tag{2}$$

the elongation rate constant is written in the general form:

$$k_+ = \Gamma_+ e^{-\frac{\Delta G_+^\ddagger}{RT}} = \Gamma_+ e^{-\frac{\Delta H_+^\ddagger - T\Delta S_+^\ddagger}{RT}} = \Gamma_+ e^{\frac{\Delta S_+^\ddagger}{R}} e^{-\frac{\Delta H_+^\ddagger}{RT}} \tag{3}$$

It can therefore be seen that the kinetic pre-factor $\Gamma_+$ and the entropy of activation $\Delta S_+^\ddagger$ are not independent of each other. One of these two parameters must be fixed in order to be able to define the other. We have in the past presented an analytical framework for the estimation of the pre-factor, based on a combination of translational and internal motion of the incorporating monomer[3]. Recently, we have presented a simplified framework where we approximate the pre-factor of the elongation rate constant by the diffusional arrival frequency of the monomer in a reaction volume at the fibril end [4], corresponding to the maximal possible rate, $r_{max} = 1.8{\cdot}10^9$ $(mol/l)^{-1}$ $s^{-1}$. We therefore use this value for the pre-factor of the elongation rate. The actual rate of attempts of crossing the free energy barrier for fibril elongation is likely significantly lower and the difference factor is hidden inside the entropy of activation for fibril elongation. We also note that in our analysis, we neglect the temperature dependence of the pre-factors for both elongation and dissociation. In particular the diffusional pre-factor for elongation can be expected to display a temperature-dependence, because the translational diffuson coefficient is temperature dependent, explicitly, as well as through its dependence on solvent viscosity.

### *2.2. Fibril dissociation*

A similar discussion applies to the dissociation of fibrils. Here the rate of dissociation of a population of fibrils is given by:

$$\frac{dM}{dt} = -k_-[P] \tag{4}$$

where k$_-$ is the dissociation rate constant with units of [s$^{-1}$]. Normalised by the concentration of fibril ends, we obtain

$$\frac{dM}{[P]dt} = -k_- \tag{5}$$

the dissociation rate constant is written in the general form:

$$k_- = \Gamma_- e^{-\frac{\Delta G^\ddagger_-}{RT}} = \Gamma_- e^{-\frac{\Delta H^\ddagger_- - T\Delta S^\ddagger_-}{RT}} = \Gamma_- e^{\frac{\Delta S^\ddagger_-}{R}} e^{-\frac{\Delta H^\ddagger_-}{RT}} \tag{6}$$

Now to the value of the pre-factor of the dissociation rate. The dissociation of a monomer from the fibril end corresponds to a barrier crossing event as outlined in Kramer's theory[5], i.e. the diffusional escape from a metastable state. In the limit of high solvent friction, the rate is given by:

$$\text{rate} = \frac{2\pi\omega_0\omega_r}{\gamma} e^{-\frac{E}{RT}} \tag{7}$$

where $\omega_0$ and $\omega_r$ are the curvatures of the potential energy at the bottom of the well and the barrier top, respectively. $\gamma = \frac{k_B T}{D}$ is the friction coefficient and E is the potential energy barrier to be overcome. In the limit of low friction, the expression simplifies further

$$\text{rate} = \frac{\omega_0}{2\pi} e^{-\frac{E}{RT}} \tag{8}$$

which corresponds to the result of transition state theory. We do not know the energy landscape in detail and hence determination of the frequencies $\omega$ is difficult. We can, however, provide a very crude estimate as the frequency of vibration of a monomer at the fibril end around its equilibrium position. Phononic frequencies have to our knowledge not been reported for amyloid fibrils, but the inter- and intramolecular vibrations of protein crystals are on the order of low THz frequencies [6]. Protein molecules inside a crystal are likely to be less strongly bound than inside an amyloid fibril. However, the monomer at the fibril end might be less strongly bound than the molecules inside the fibril and therefore experience a comparable restoring force towards its equilibrium

position. We therefore approximate the attempt frequency for fibril dissociation with 1 THz, corresponding to a pre-factor of $10^{12}\mathrm{s}^{-1}$.

## 3. Temperature jump experiments of amyloid fibril growth and dissociation

Here we are discussing the following experiment. Take amyloid fibrils at equilibrium at a temperature $\mathrm{T}_1$ and subject them to a rapid temperature jump to a new temperature $\mathrm{T}_2$, with $\mathrm{T}_2 > T_1$. The equilibrium monomer concentration, also referred to as the critical concentration $\mathrm{c}_{\mathrm{crit}}$, will be higher at $\mathrm{T}_2$ than at $\mathrm{T}_1$. Therefore, immediately after the temperature jump, the system will be out of equilibrium and the fibrils need to dissociate to some extent to establish a new equilibrium. We are interested in the rate of relaxation of the system to equilibrium and if and how we can extract the dissociation rate constant from this relaxation process. Let us assume the number concentration of active fibril ends, P, does not change during the process. The differential equation governing the change in monomer concentration is given by:

$$\frac{d[m](t)}{dt} = -k_+[P][m](t) + k_-[P] \tag{9}$$

The monomer concentration can be written as

$$[m](t) = m_{\mathrm{eq}}(T_2) + [\Delta m](t) \tag{10}$$

whereby $m_{\mathrm{eq}}(T_2) = c_{\mathrm{crit}}$ is the equilibrium monomer concentration at temperature $\mathrm{T}_2$, and $[\Delta m](t)$ is the deviation from equilibrium. For the specific T-jump experiment considered here, i.e. jump to a higher temperature, $[\Delta m](t)$ is negative.

For simplicity, we absorb the fibril end concentration [P] into the rate constants, according to

$$k_i[P] = k_i'. \tag{11}$$

We insert equation 2 into equation 1 and observe that the time derivative of the equilibrium concentration is zero:

$$\frac{d[\Delta m](t)}{dt} = -k'_+(m_{\mathrm{eq}}(T_2) + [\Delta m](t)) + k'_- \tag{12}$$

or

$$\frac{d[\Delta m](t)}{dt} + k'_+[\Delta m](t) = k'_- - k'_+ m_{\mathrm{eq}}(T_2) \tag{13}$$

The general solution to this inhomogeneous linear differential equation is given by the sum of the solutions to the homogeneous equation:

$$[\Delta m](t) = Ae^{-k'_+ t} + B \tag{14}$$

and a particular solution:

$$[\Delta m](t) = \frac{k'_-}{k'_+} - m_{\mathrm{eq}}(T_2) \tag{15}$$

we therefore obtain:

$$[\Delta m](t) = Ae^{-k'_+ t} + B + \frac{k'_-}{k'_+} - m_{\mathrm{eq}}(T_2) \tag{16}$$

if we use the boundary conditions $[\Delta m](0) = [\Delta m]_0$ (corresponding to the amplitude of the jump in critical concentration) and $[\Delta m](\infty) = 0$, we can determine the constants A and B by using the relationship

$$\frac{k'_-(T_2)}{k'_+(T_2)} = m_{\mathrm{eq}}(T_2) \tag{17}$$

to be $\mathrm{A} = [\Delta m]_0$ and $\mathrm{B} = 0$. We therefore finally obtain:

$$[\Delta m](t) = [\Delta m]_0 e^{-k'_+ t} \tag{18}$$

This result implies that amyloid fibril growth always relaxes with the elongation rate constant as exponential decay constant, because only elongation is concentration-dependent. Any information on the dissociation rate constants is hidden in the $[\Delta m]_0$.

For our example, a jump from $T_1$ to $T_2$, with $T_2 > T_1$, the system was at equilibrium at $T_1$ before the T-jump. Therefore, $[\Delta m]_0 = m_{\mathrm{eq}}(T_1)\text{-}m_{\mathrm{eq}}(T_2) = \frac{k'_-(T_1)}{k'_+(T_1)} - \frac{k'_-(T_2)}{k'_+(T_2)} < 0$.

We now Taylor expand the expression for the relaxation of $[\Delta m](t)$ and keep only the linear term:

$$[\Delta m](t) = [\Delta m]_0 e^{-k'_+(T_2)t} \approx [\Delta m]_0(1 - k'_+(T_2)t) \tag{19}$$

and therefore the slope right after the T-jump:

$$\left.\frac{d[\Delta m](t)}{dt}\right|_0 \approx -[\Delta m]_0 k'_+(T_2) = k'_-(T_2) - \frac{k'_-(T_1)k'_+(T_2)}{k'_+(T_1)} \tag{20}$$

Therefore, the temperature dependence of the dissociation rate can be extracted from T-jump experiments if both the magnitude of the jumps in concentration, as well as the temperature-dependence of the growth rate are known. This is equivalent to saying that if we know the temperature dependence of the equilibrium/critical concentration (analogous to a van't Hoff analysis, as well as the temperature-dependence of the growth rate, we can obtain the temperature-dependence of the dissociation rate. An approximate value of the dissociation rate constant can also be obtained by measuring the initial slope of the dissociation upon a jump to a higher temperature. As can be seen from equation 20, the slope is approximately equal to the dissociation rate constant at the higher temperature. For situations where large temperature jumps are performed which increase the dissociation constant several fold, and if the temperature dependence of the dissociation rate constant is significantly larger than that of the elongation rate constant, the correction term $\frac{k'_-(T_1)k'_+(T_2)}{k'_+(T_1)}$ is small. However, this correction term decreases with increasing $T_2$ and therefore the slope of an Arrhenius plot based on the initial slopes of the dissociation will lead to an underestimation of the true temperature dependence. In order to perform the correction formally on the Arrhenius-plot obtained from the initial slopes, we re-write equation 20 as:

$$\left.\frac{d[\Delta m](t)}{dt}\right|_0 \approx k'_-(T_2)\left(1-\frac{k'_-(T_1)k'_+(T_2)}{k'_-(T_2)k'_+(T_1)}\right) = k'_-(T_2)\left(1-e^{\frac{\Delta H^\ddagger_-}{R}\left(\frac{1}{T_2}-\frac{1}{T_1}\right)}e^{\frac{\Delta H^\ddagger_+}{R}\left(\frac{1}{T_1}-\frac{1}{T_2}\right)}\right) \tag{21}$$

We can perform the correction iteratively, by fixing $\Delta H^\ddagger_+$ to the value determined from the other experiment and we use as a first approximation for $\Delta H^\ddagger_-$ the value determined from the un-corrected analysis of the initial slopes. Calculation of the correction factor then yields a better approximation of $\Delta H^\ddagger_-$.

## 4. Arrhenius analysis of rates vs. rate constants

In Arrhenius analysis, the temperature dependence of the kinetics of a reaction is investigated with the aim to define the energy barriers of the reaction. In [4], we have given a detailed description as to the relationship between the Arrhenius activation energy and the enthalpy of activation, which are very similar. Arrhenius analysis is normally carried out on the rate constants of a reaction. However, in most cases where the temperature-dependence of amyloid fibril growth has been studied, and an Arrhenius analysis has been carried out, the rates of fibril growth have been plotted against inverse absolute temperature, and the Arrhenius activation energy of the elongation step has been extracted from a linear fit to this data, according to:

$$\frac{d(\text{rate})}{d\left(\frac{1}{T}\right)} = \frac{d\left(\frac{d[M]}{dt}\right)}{d\left(\frac{1}{T}\right)} = \frac{d(k_+[P][m])}{d\left(\frac{1}{T}\right)} = -\frac{E_A}{RT} \approx -\frac{H^\ddagger}{RT} \tag{22}$$

This type of analysis assumes that the rate of fibril growth is always proportional to the rate constant. This is valid as long as only the process of elongation is studied in isolation, both in the low concentration regime, where the growth rate is proportional to monomer concentration, as well as in the high concentration regime, where the growth rate becomes independent of monomer concentration[4]. Indeed, we have found in the past that the slopes of Arrhenius plots in both the low and high concentration regimes are parallel[3]. However, as soon as fibril dissociation contributes significantly, this proportionality no

longer holds. The general expression if both growth and dissociation contribute to the dynamics of fibril mass is given by:

$$\frac{d(\text{rate})}{d\left(\frac{1}{T}\right)} = \frac{d\left(\frac{d[M]}{dt}\right)}{d\left(\frac{1}{T}\right)} = \frac{d(k_+[P][m] - k_-[P])}{d\left(\frac{1}{T}\right)} \tag{23}$$

In the limit of negligible dissociation rate $k_-$, this expression reduces to equation 21. The balance between fibril growth and dissociation at any given temperature depends on the monomer concentration, and hence it is easy to understand that an Arrhenius-plot constructed in this way, i.e. with rates, rather than rate constants plotted, will possibly show a concentration dependence. This concentration dependence manifests itself in a concentration dependent curvature of the Arrhenius-plot at high temperatures, where the dissociation rate becomes non-negligible (T>40℃ for PI3K-SH3 under the conditions of this study). Supplementary Figure 1, illustrates this concept, even though the data is plotted linearly and not as an Arrhenius-plot.

It is therefore advantageous to use a method that allows to directly extract the rate constant, such as the perturbation (T-jump) approach developed in the present work and discussed in Appendix 2.

## 5. The critical concentration of amyloid fibril growth

The simplest model to describe the thermodynamics of amyloid fibril formation is the isodesmic linear polymerisation model, in which amyloid fibril formation is described as a series of infinite equilibria of monomer additions, all with the same equilibrium constant [7, 8, 9]. Mathematical treatment of this model leads to the following relationship between the equilibrium constant and the monomer concentration at equilibrium [10]:

$$K = \frac{m_0}{[m]} - \sqrt{\frac{m_0^2}{[m]M_{\text{tot}}}} \tag{24}$$

where $m_0$ is a standard concentration to make the expression unit-less and $M_{\text{tot}}$ is the total monomer equivalent concentration, including soluble and fibril-

lar protein. If the free monomer concentration [m]$\ll$M$_{\mathrm{tot}}$, then this expression simplifies to:

$$K \approx \frac{m_0}{[m]} \tag{25}$$

The same expression can be obtained if we assume an equilibrium between fibril growth and dissociation for constant number of fibril ends:

$$k_+[P][m] = k_-[P] \tag{26}$$

and therefore

$$K = \frac{k_-[P]}{k_+[P]} = \frac{k_-}{k_+} = \frac{m_0}{[m]} \tag{27}$$

Therefore, the monomer concentration at equilibrium is a measure for the affinity of the monomer for the fibril end. However, it is not straightforward to apply this concept to full thermal denaturation curves of amyloid fibrils. When a given concentration of amyloid fibrils is heated up slowly enough for the system to equilibrate, then the monomer concentration can be initially used to define the stability of the fibrils at a given temperature. However, as [m] approaches M$_{\mathrm{tot}}$, the correction term in equation 23 becomes more significant and can no longer be neglected. This means that the equilibrium monomer concentration is no longer independent of the total concentration, but varies according to [9]:

$$[m] = \frac{1}{K} + \frac{1}{2K^2[M]_{tot}} - \sqrt{\frac{1}{K^3[M]_{tot}} + \frac{1}{4K^4[M]_{tot}^2}} \tag{28}$$

A fit to the spectroscopically (DSF) determined soluble protein concentration at equilibrium as a function of total concentration to this equation is shown in supplementary figure 4. The critical concentration at 60℃ can be estimated to be of the order of 15 $\mu$M. At higher temperatures, the total concentration, M$_{\mathrm{tot}}$, is not high enough to allow an accurate estimate of c$_{\mathrm{crit}}$.

Furthermore, in this regime, the number of fibrils is no longer constant and the fibrils become shorter and shorter. This slows down the rate of dissociation

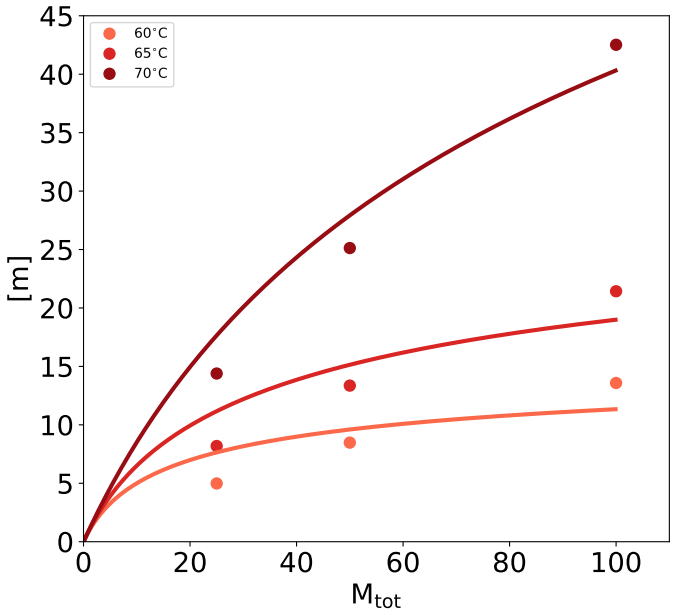


Figure 4: Equilibrium monomer concentrations estimated from DSF experiments, as a function of temperature and total protein concentration in the sample.

and therefore equilibration, and can also lead to practical problems of measuring the concentration of monomer by spectroscopy, as the spectroscopic signature of very short fibrils/oligomers might be more similar to that of monomers compared to the spectroscopic signature of full length fibrils. Lastly, it has to be noted that the isodesmic linear polymerisation model is not able to describe the full complexity of the concentration and denaturant dependence of amyloid fibril stability, but that the nucleated polymerisation model provides a better description [9].

## 6. Temperature ramping experiments

To extract the concentration of monomeric protein during the temperature ramping experiments of PI3K-SH3 fibrils, the temperature dependence of the

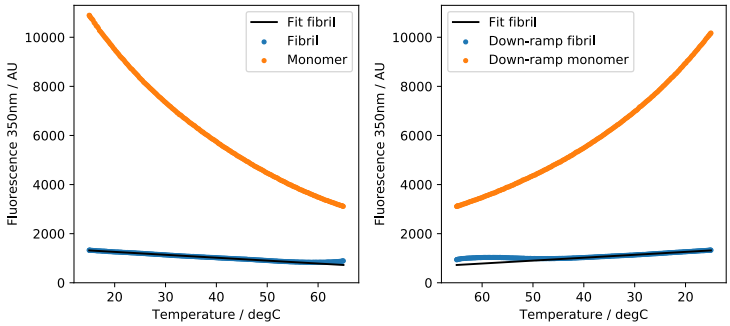


Figure 5: Example of raw data used to extract the fraction of monomeric protein for the temperature ramp experiments. Here, data is shown for the ramping at 1℃/minute from 15 to 65℃ (left) and down again (right) using a 100 $\mu M$ sample.

fibril fluorescence (base-line), $f_{bl}$, at 350 nm was modelled by a linear function from 15℃ to 50℃ (Figure 5). Extrapolating this model to the remaining temperature range where dissociation was observed allowed for a calculation of the monomer concentration $[m]$:

$$[m] = \frac{f_{350nm} - f_{bl}}{m_{bl} - f_{bl}} \cdot c_{total} \tag{29}$$

Where, $f_{350nm}$ is the fluorescence intensity of the fibril sample at 350 nm, $m_{bl}$ is the fluorescence intensity of the fully monomeric sample, and $c_{total}$ is the total concetration of protein in the fibril sample. The monomeric sample was prepared by fully denaturing the same solution at 90℃ to ensure exactly the same concentration.

The temperature ramping experiments were fitted to a model of the following form:

$$\frac{d[m]}{dt} = k'_{-}(t) - k'_{+}[m](t) = \Gamma_{-} e^{-\frac{\Delta H^{\ddagger}_{-} - (T_0 + a(t)t)\Delta S^{\ddagger}_{-}}{R(T_0 + a(t)t)}}[P] - \Gamma_{+} e^{-\frac{\Delta H^{\ddagger}_{+} - (T_0 + a(t)t)\Delta S^{\ddagger}_{+}}{R(T_0 + a(t)t)}}[P][m] \tag{30}$$

where a(T) is the slope of the temperature ramp. In the ramp shown in figure 3 of the main manuscript, a(T) has initially a positive value (0.5, 1 or 1.5℃/min),

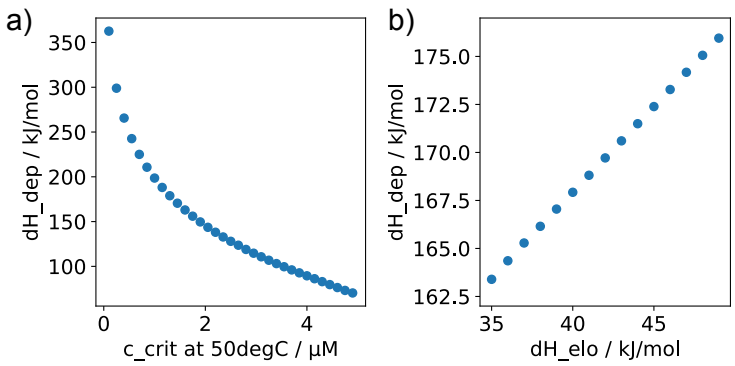


Figure 6: Sensitivity of the activation enthalpy of the dissociation reaction extracted from T-ramp experiments as a) choice of critical concentration at 50°C and b) choice of fixed value for the enthalpy of activation of the growth reaction.

then for technical reasons becomes 0 for approximately 90s, and then switches sign to become negative (-0.5, -1 or -1.5°C/min). There appears to be no general analytical solution to this differential equation and therefore we fitted the data numerically with Python. In order for the fit to yield consistent values, we found it necessary to impose a boundary condition in the form of a constraint that fixes the equilibrium monomer concentration at a given temperature to a known value. Due to the uncertainty associated with determining the critical concentration directly (see section above), we used the estimate of the critical concentration at 50°C from the QCM experiments in supplementary figure 2, i.e.:

$$c_{\mathrm{crit}}(50) = \frac{k_-(50°C)}{k_+(50°C)} = 1.5 \cdot 10^{-6} M \tag{31}$$

In addition, we also found it necessary to fix the value of the activation enthalpy of the elongation reaction. we varied its value within the full range of plausible values determined in this study (ca. 35 to 50 kJ/mol). The resulting activation enthalpy for the dissociation reaction was found to be rather sensitively dependent on both the imposed $\Delta H_+^{\ddagger}$ as well as the imposed constraint for the equilibrium concentration at 50°C (see supplementary figure 6).

For the calculation of the thermodynamic stability of the fibrils at 28℃, we used $\Delta H_{+}^{\ddagger} = 40$ kJ/mol and $c_{crit}(50°C) = \frac{k_{-}(50°C)}{k_{+}(50°C)} = 1.5{\cdot}10^{-6}$M.

## References


[1] T. C. T. Michaels, A. K. Buell, E. M. Terentjev, T. P. J. Knowles, Quantitative analysis of diffusive reactions at the solid–liquid interface in finite systems, J. Phys. Chem. Lett. 5(4) (2014) 695–699.

[2] A. K. Buell, A. Dhulesia, D. A. White, T. P. J. Knowles, C. M. Dobson, M. E. Welland, Detailed analysis of the energy barriers for amyloid fibril growth., Angew Chem Int Ed Engl 51 (21) (2012) 5247–5251. doi:10.1002/anie.201108040.
URL http://dx.doi.org/10.1002/anie.201108040

[3] A. K. Buell, J. R. Blundell, C. M. Dobson, M. E. Welland, E. M. Terentjev, T. P. J. Knowles, Frequency factors in a landscape model of filamentous protein aggregation., Phys Rev Lett 104 (22) (2010) 228101.

[4] A. K. Buell, The growth of amyloid fibrils: rates and mechanisms, Biochemical Journal 476 (19) (2019) 2677–2703.

[5] H. A. Kramers, Brownian motion in a field of force and the diffusion model of chemical reactions, Physica 7 (1940) 284–304.

[6] G. Acbas, K. A. Niessen, E. H. Snell, A. Markelz, Optical measurements of long-range protein vibrations, Nature communications 5 (1) (2014) 1–7.

[7] T. Narimoto, K. Sakurai, A. Okamoto, E. Chatani, M. Hoshino, K. Hasegawa, H. Naiki, Y. Goto, Conformational stability of amyloid fibrils of beta2-microglobulin probed by guanidine-hydrochloride-induced unfolding., FEBS Lett 576 (3) (2004) 313–319. doi:10.1016/j.febslet.2004.09.024.
URL http://dx.doi.org/10.1016/j.febslet.2004.09.024

[8] A. J. Baldwin, T. P. J. Knowles, G. G. Tartaglia, A. W. Fitzpatrick, G. L. Devlin, S. L. Shammas, C. A. Waudby, M. F. Mossuto, S. Meehan, S. L. Gras, J. Christodoulou, S. J. Anthony-Cahill, P. D. Barker, M. Vendruscolo, C. M. Dobson, Metastability of native proteins and the phenomenon of amyloid formation., J Am Chem Soc 133 (36) (2011) 14160–14163. doi:10.1021/ja2017703.
URL http://dx.doi.org/10.1021/ja2017703

[9] N. Vettore, A. K. Buell, Thermodynamics of amyloid fibril formation from chemical depolymerization, Physical Chemistry Chemical Physics 21 (47) (2019) 26184–26194.

[10] A. K. Buell, C. M. Dobson, M. E. Welland, Amyloid Proteins - Methods and Protocols, 2nd Edition, Vol. 849 of Methods in Molecular Biology, Humana Press, 2012.